Article:
Verzella, D, Bennett, J, Fischietti, M et al. (17 more authors) (2018) GADD45β Loss Ablates Innate Immunosuppression in Cancer. Cancer Research, 78 (5). pp. 1275-1292. ISSN 0008-5472

https://doi.org/10.1158/0008-5472.CAN-17-1833

Author Manuscript Published OnlineFirst on December 26, 2017; DOI: 10.1158/0008-5472.CAN-17-1833
Author manuscripts have been peer reviewed and accepted for publication but have not yet been edited.

GADD45β loss ablates innate immunosuppression in cancer

Daniela Verzella[1,9], Jason Bennett[2,9], Mariafausta Fischietti[1,9], Anil K. Thotakura[2,9], Camilla Recordati[3], Fabio Pasqualini[4], Daria Capece[1], Davide Vecchiotti[1], Daniel D'Andrea[2], Barbara Di Francesco[1], Marcella De Maglie[3], Federica Begalli[2], Laura Tornatore[2], Salvatore Papa[2,5], Toby Lawrence[6], Stuart J. Forbes[7], Antonio Sica[4,8], Edoardo Alesse[1], Francesca Zazzeroni[1,10,*], and Guido Franzoso[2,10,*]

[1]Department of Biotechnological and Applied Clinical Sciences, University of L'Aquila, 67100 L'Aquila, Italy

[2]Centre for Cell Signalling and Inflammation, Department of Medicine, Imperial College London, London W12 0NN, UK

[3]Mouse & Animal Pathology Laboratory, Fondazione Filarete, 20139, Milan, Italy

[4]Department of Inflammation and Immunology, Humanitas Clinical and Research Center, Rozzano, Milan 20089, Italy

[5]Current address: Leeds Institute of Cancer and Pathology (LICAP), University of Leeds, Leeds, LS9 7TF, UK

[6]Centre d'Immunologie de Marseille-Luminy, Aix Marseille Université, Inserm, CNRS, 13288 Marseille, France

[7]Medical Research Council Centre for Regenerative Medicine, University of Edinburgh, Edinburgh EH16 4UU, UK

[8]Department of Pharmaceutical Sciences, Università del Piemonte Orientale 'Amedeo Avogadro', via Bovio 6, Novara 20089, Italy

[9]Joint first author

[10]Co-last author

[*]Correspondence:

Guido Franzoso, Centre for Cell Signalling and Inflammation, Imperial College London, Room 10N8, Commonwealth Building, Hammersmith Campus, Du Cane Road, London, W12 0NN, UK; e-mail address: g.franzoso@imperial.ac.uk

Francesca Zazzeroni, Department of Biotechnological and Applied Clinical Sciences, University of L'Aquila, Via Vetoio 10 – Coppito II, 67100 L'Aquila, Italy; e-mail address: francesca.zazzeroni@univaq.it

RUNNING TITLE

Breaking cancer immunosuppression via GADD45β deletion

KEYWORDS

GADD45β, NF-κB, Inflammation, Tumour associated macrophage (TAM), Tumour microenvironment (TME).

FINANCIAL SUPPORT

The work was supported in part by Cancer Research UK programme grant A15115, Medical Research Council (MRC) Biomedical Catalyst grant MR/L005069/1 and Bloodwise project grant 15003 to G.F., the Associazione Italiana per la Ricerca sul Cancro (AIRC) grants 1432 and 5172 and MIUR PRIN grant n° 2009EWAW4M_003 to F.Z., MIUR FIRB grant n° RBAP10A9H9 to E.A., and the Associazione Italiana per la Ricerca sul Cancro (AIRC) grant 15585 to A.S.

COMPETING FINANCIAL INTERESTS

The authors declare no competing financial interests.

DISCLOSURE OF CONFLICTS OF INTEREST

The authors declare no conflicts of interest.

ABSTRACT

T cell exclusion from the tumour microenvironment (TME) is a major barrier to overcoming immune escape. Here we identify a myeloid-intrinsic mechanism governed by the NF-κB effector molecule GADD45β that restricts tumour-associated inflammation and T cell trafficking into tumours. In various models of solid cancers refractory to immunotherapies, including hepatocellular carcinoma (HCC) and ovarian adenocarcinoma, *Gadd45b* inhibition in myeloid cells restored activation of pro-inflammatory tumour-associated macrophages (TAM) and intratumoural immune infiltration, thereby diminishing oncogenesis. Our results provide a basis to interpret clinical evidence that elevated expression of GADD45B confers poor clinical outcomes in most human cancers. Further, they suggest a therapeutic target in GADD45β for re-programming TAM to overcome immunosuppression and T cell exclusion from the TME.

PRECIS

Findings define a myeloid-based immune checkpoint that restricts T cell trafficking into tumours, with potentially important therapeutic implications to generally improve the efficacy of cancer immunotherapy.

INTRODUCTION

Virtually all tumours contain an inflammatory infiltrate of innate and adaptive immune cells (1). Despite their inherent capacity to counter neoplastic progression and eliminate nascent tumours, these cells – especially those of the innate immune system – often have the effect of promoting oncogenesis (1,2). Accordingly, tumour-

associated inflammation is now considered a hallmark of cancer (1). The ability of the immune system to influence oncogenesis is currently being exploited to treat cancer patients, with the development of many successful anticancer immunotherapies (3). Indeed, therapies blocking pivotal immunoinhibitory mechanisms, comprising immune checkpoint molecules, *e.g.*, cytotoxic T lymphocyte antigen-4 (CTLA-4) or programmed cell death protein 1 (PD-1), are revolutionising the clinical management of certain malignancies, such as metastatic melanoma (4). However, major challenges remain, as the majority of patients rarely exhibit an objective response to these treatments, due to the absence of a pre-existing intratumoural T-cell infiltrate or, in patients with T-cell-infiltrated tumours, the dominant inhibitory effects of additional tumour microenvironment (TME)-associated molecules (3,5). Yet, the mechanisms underlying the immunoinhibitory activities of the TME are presently poorly understood.

Tumour-associated macrophages (TAMs) are implicated in various TME-mediated mechanisms that enable cancers to evade immune attack (3,6,7). TAMs are the main leukocyte population found in most human tumours, where they play a key role in restricting local T-cell trafficking and T-cell effector functions (3,6,7). Indeed, a high density of TAMs, especially those exhibiting an antiinflammatory and immunosuppressive phenotype, correlates with poor clinical outcome in most human cancers (7,8). Accordingly, therapeutic approaches limiting myeloid cell recruitment into tumours have resulted in increased TME-based $CD8^+$ effector T-cell infiltration and diminished tumour burden in mouse models and early-phase clinical trials (3,6,9-13). However, the general macrophage depletion associated with these approaches raises important safety concerns. Therefore, a preferable approach would be to reprogramme TAMs toward a proinflammatory phenotype capable of redirecting T-cell trafficking into tumours and unleashing local antitumour immune responses (6,14).

Macrophages can differentiate into a spectrum of phenotypic states in response to diverse environmental signals. At sites of infection, “classically” activated or proinflammatory macrophages (hereafter also occasionally referred to as M1-like marophages) arise in response to interferon-γ (IFN-γ) and TolI-like receptor (TLR) ligands to eliminate invading pathogens, promote inflammation and engage the adaptive immune system. By contrast, “alternatively” activated or antiinflammatory macrophages (hereafter also occasionally referred to as M2-like marophages) are “educated” by interleukin-4 (IL-4) and IL-13 at sites of injury to terminate inflammation and enable wound healing (7,8). Interestingly, antiinflammatory macrophages resemble the TAMs found in most human cancers, where they support tumour progression, metastatic dissemination and cancer immune evasion (7,8). However, little is known about the mechanisms governing the opposing functions of macrophages in response to tissue injury, malignancy or infection. Consequently, there are presently no therapeutic agents capable of effectively reprogramming TAMs to oppose oncogenesis.

Recent studies have identified NF-κB transcription factors as key determinants in the balance between proinflammatory and antiinflammatory macrophage activation in response to infection or tumour-derived signals (15,16). In fact, in addition to orchestrating protective immune and inflammatory responses, the NF-κB pathway drives oncogenesis in multiple cancer types by suppressing apoptosis of tumour cells and, concurrently, governing TME-based inflammation, thereby serving as a central hub linking cancer and inflammation (16,17). In ovarian adenocarcinoma models, macrophage-specific inhibition of the NF-κB-activating kinase, IκBα kinase (IKK)β, was shown to reverse the antiinflammatory TAM phenotype and enhance proinflammatory macrophage activation, thereby causing tumour regression (18). A similar conversion from an antiinflammatory TAM activation state supportive of oncogenesis to a proinflammatory activation state that

antagonises tumour growth, was reported in melanoma and fibrosarcoma models, in mice bearing TAMs lacking NF-κB1/p105 (19). Notably, this IKKβ/NF-κB function in suppressing proinflammatory activation was shown to extend beyond the cancer context, reflecting the tissue-specific role that IKKβ/NF-κB plays in myeloid cells, where opposite to its conventional proinflammatory role, NF-κB drives the resolution of inflammation to enable wound healing and prevent tissue damage (20,21).

Therefore, the IKKβ/NF-κB pathway provides an attractive route to therapeutically reverse TME-mediated immunosuppression by reprogramming TAMs toward a proinflammatory phenotype (15,18). However, therapeutically targeting this pathway with conventional IKKβ/NF-κB inhibitors has not proven possible, due to the severe on-target toxicities associated with globally suppressing NF-κB (17). A logical alternative to pharmacologically inhibiting IKKβ/NF-κB would be therefore to target the non-redundant downstream effectors of the NF-κB antiinflammatory function in myelo-monocytic cells. However, these effectors and their modes of action remain poorly understood.

Here, we report that the NF-κB-regulated protein, GADD45β (22,23), mediates an essential myeloid-intrinsic mechanism governing proinflammatory macrophage activation and the immunosuppressive activity of the TME that restrict $CD8^+$ T-cell trafficking into tumours. Using three distinct models of solid cancers that are largely refractory to immunotherapies, including hepatocellular carcinoma (HCC) and ovarian adenocarcinoma, we showed that *Gadd45b* deletion in myeloid cells restores proinflammatory TAM activation and intratumoural $CD8^+$ T-lymphocyte infiltration, resulting in diminished tumour growth. Since we previously showed that GADD45β additionally mediates the NF-κB antiapoptotic activity in cancer cells (24), our current findings identify GADD45β as a pivotal downstream hub integrating the NF-κB oncogenic functions linking cancer and inflammation. Our finding that elevated *GADD45B* expression correlates with poor clinical outcomes across most

human cancers consolidates the general clinical significance of the GADD45β-mediated oncogenic mechanism in malignant disease. Together, these results reveal a pathogenically critical, innate immunity "checkpoint" governed by GADD45β that is amenable to therapeutic intervention to "re-educate" TAMs and ultimately overcome TME-dependent immunosuppression, with profound implications for anticancer therapy.

MATERIALS AND METHODS

Human Cancer Datasets

The human datasets of lung cancer (LUNG), stomach adenocarcinoma (STAD), non-alcoholic liver hepatocellular carcinoma (LIHC), esophageal carcinoma (ESCA), cervical carcinoma (CESC), untreated primary glioblastoma multiforme (GBM), cholangiocarcinoma (CHOL), head and neck squamous cell carcinoma (HNSC) and kidney clear cell carcinoma (KIRC) were part of The Cancer Genome Atlas (TCGA) (25) programme and downloaded from the UCSC Cancer Genomic Browser (26). Gene expression profiling was performed on fresh or frozen tissue biopsies using the Illumina HiSeq 2000 RNA Sequencing platform. The estimates of *GADD45B* expression levels were derived from the normalised values in the UCSC Cancer Genomic Browser. The datasets of colon adenocarcinoma (COAD; GSE39582), bladder carcinoma (BLCA; GSE13507) and ovarian cancer (OV; GSE9891) were deposited in the National Center for Biotechnology Information (NCBI) Gene Expression Omnibus (GEO) database (www.ncbi.nlm.nih.gov/geo). The COAD dataset was from the French national Cartes d'Identité des Tumeurs (CIT) programme and generated using the Affymetrix Human Genome U133 Plus 2.0

Array platform (27). The BLCA dataset was from the Chungbuk National University Hospital and generated using the Illumina human-6 v2.0 expression beadchip platform (28). The OV dataset was from the Australian Ovarian Cancer Study, Royal Brisbane Hospital, Westmead Hospital, and Netherlands Cancer Institute and generated using the Affymetrix Human Genome U133 Plus 2.0 Array platform (29). The relative *GADD45B* mRNA expression levels in these datasets were derived from the normalised values present in the GEO database. The breast carcinoma dataset (BRCA) was from the tumour banks in the UK and Canada, and gene profiling data were generated using the Illumina HumanHT-12 V3 platform and deposited on Oncomine® Research Premium Edition (30).

The gene profiling data from each dataset were downloaded together with the accompanying clinical information. Where possible, the series were obtained from patients at an early disease stage and datasets with a sufficient number of patients with Recurrence Free Survival (RFS) information. In the other cases, where this was not possible, the series consisted of Overall Survival (OS) data and/or the entire patient dataset. Patients were stratified into two groups on the basis of the *GADD45B* mRNA expression levels. In each case, quintiles, quartiles, tertiles and 95th percentiles were used as thresholds, and the best fits are reported in Figure 1A-1M.

Cell Culture and Macrophage Isolation and Treatment

The C57BL/6 mouse fibrosarcoma cell line, MCA-203 was kindly provided by I. Marigo and V. Bronte and cultured in high-glucose Dulbecco's modified Eagle's medium (DMEM; with L-glutamine, without sodium pyruvate; Gibco) supplemented with 10% heat-inactivated fetal bovine serum (FBS; Sigma-Aldrich), antibiotics (150 U/mL penicillin, 200 U/mL streptomycin), 10 mM HEPES (Gibco), 2 μM β-

mercaptoethanol and 2 mM L-glutamine (Gibco). The C57BL/6 mouse ovarian carcinoma cell line, ID8-Luc, stably expressing firefly luciferase (Luc), was previously described (18) and cultured in high-glucose DMEM (with L-glutamine, without sodium pyruvate; Gibco) supplemented with 4% heat-inactivated FBS (Sigma-Aldrich), antibiotics (150 U/mL penicillin, 200 U/mL streptomycin), ITS+1 Liquid Media Supplement (5 µg/ml insulin, 5 µg/ml transferrin, 5 ng/ml sodium selenite; Sigma-Aldrich) and 2 mM L-glutamine (Gibco). Cells were cultured in a humidified incubator in 5% CO_2 at 37°C. All cell lines were routinely tested using a Mycoplasma Detection Kit (ATCC). Before injection *in vivo*, cell lines were also routinely screened for other infectious agents using the Mouse Essential CLEAR Panel (Charles River). The cell lines authentication for the MCA-203 and ID8-Luc murine cell lines has not been possible because these cell lines are not commercially available. Cells were used for the experiments between 5 and 7 days upon thawing.

BMDMs were prepared from 6 to 10 weeks old *Gadd45b*$^{-/-}$ and *Gadd45b*$^{+/+}$ C57BL/6J mice as previously described (21). BMDMs were treated with LPS (*E. coli* serotype O55:B5, 100 ng/mL; Sigma-Aldrich) and mouse recombinant IFNγ (20 ng/mL; Sigma-Aldrich) or with mouse recombinant IL-4 (20 ng/mL; Peprotech) and mouse recombinant IL-13 (20 ng/mL; Peprotech). The p38 inhibitors used were: Vx745 (20 µM; Selleckchem); Skepinone-L (10 µM; Selleckchem); SB203580 (20 µM; Cell Signalling Technology).

For TAM isolation, intraperitoneal cells were harvested from ID8-Luc tumour-bearing mice by peritoneal lavage with 1x PBS and passed through a 70-µm cell strainer (BD Biosciences), following red blood cell removal with RBC lysis buffer (Sigma-Aldrich). TAMs were separated using MACS MicroBead™ Technology (Miltenyi Biotec) by negative selection with anti-Ly-6G MicroBead Kit, mouse, followed by positive selection with CD11b MicroBeads, human and mouse (Miltenyi Biotec), according to the manufacturer's instructions.

Further information on the procedures for BMDM isolation can be found in the Supplementary Information.

BMDM/Tumour Cell Co-Culture

Gadd45b$^{-/-}$ and *Gadd45b*$^{+/+}$ BMDMs were prepared as above and co-cultured with ID8-Luc or MCA-203 tumour cells, without direct cell-to-cell contact, according to established protocols (18,31). Further information on the procedures for BMDM/tumour cell co-culture can be found in the Supplementary Information.

Mice

C57BL/6Jx129/SvJ *Gadd45b*$^{-/-}$ mice were previously described (32). *Gadd45b*$^{+/+}$ littermates were co-housed and used as controls. C57BL/6J *Gadd45b*$^{-/-}$ and *Gadd45b*$^{+/+}$ mice were obtained by backcrossing the corresponding C57BL/6Jx129/SvJ lines onto C57BL/6J to at least the N14 backcross generation. C57BL/6J CD45.1/Ly5.1^{+} mice (B6.SJL-*Ptprc*^{a} *Pepc*^{b}/BoyJ) and C57BL/6J LysM-cre transgenic mice were purchased from The Jackson Laboratory. C57BL/6J *Gadd45b*$^{-/-}$ and *Gadd45b*$^{+/+}$ mice, expressing either CD45.2/Ly5.2^{+} or CD45.1/Ly5.1^{+}, were co-housed and bred as separate colonies.

Conditional *Gadd45b* knockout mice, carrying loxP-flanked *Gadd45b* alleles (*Gadd45b*^{F}), were generated at Taconic Biosciences using conventional gene targeting technology in embryonic stem (ES) cells. Homozygous *Gadd45b*$^{F/F}$ mice were obtained by the inter-breeding of *Gadd45b*$^{F/+}$ mice. *Gadd45b*$^{\Delta M/\Delta M}$ mice, specifically lacking *Gadd45b* in the myeloid lineage, were generated by crossing *Gadd45b*$^{F/F}$ mice with C57BL/6J LysM-cre mice (The Jackson Laboratory), expressing a Cre recombinase transgene under the control of the myeloid-specific

LysM promoter (33). Co-housed *Gadd45b*$^{F/F}$ littermates were used as controls for the experiments.

Mice were housed in ventilated cages in a pathogen-free mouse facility of the Central Biomedical Services at Imperial College London and used in accordance with established institutional guidelines, under the authority of UK Home Office project license, P75F16A53 (see: Guidelines on the Operation of Animals [Scientific Procedures] Act of 1986). Separate mouse colonies were maintained in filtered top cages on autoclaved food, water and bedding in the Conventional Mouse Facility at the University of L'Aquila, and experimental procedures were performed in accordance with national and international laws and regulations (see: European Economic Community Council Directive 86/609, OJ L 358, 1, December 12, 1987; Italian Legislative Decree 116/92, Gazzetta Ufficiale della Republica Italiana no.40, February 18, 1992; National Institutes of Health Publication no.85-23, 1985), under the approval of the University of L'Aquila Internal Committee and the Italian Ministry of Health.

Further information on the procedures used for the generation of *Gadd45b*$^{F/F}$ mice can be found in the Supplementary Information.

BM Chimaeras

Congenic CD45.1/Ly5.1^{+} *Gadd45b*$^{-/-}$ and *Gadd45b*$^{+/+}$ mice were generated by crossing the corresponding C57BL/6J lines (CD45.2/Ly5.2^{+}) with C57BL/6J B6.SJL-*Ptprc*^{a} *Pepc*^{b}/BoyJ mice (The Jackson Laboratory), carrying homozygous *Ptprc*^{a} (*CD45.1/Ly5.1*) alleles, and used as donors in BM adoptive transfer experiments to distinguish between haematopoietic-derived cells of recipient (CD45.2/Ly5.2^{+}) and donor (CD45.1/Ly5.1^{+}) origin. For these experiments, BM cells were harvested from femurs and tibiae of 6 to 10 weeks old CD45.1/Ly5.1^{+} *Gadd45b*$^{-/-}$ or *Gadd45b*$^{+/+}$

males under aseptic conditions. Red blood cells were lysed using RBC lysis buffer (Sigma-Aldrich), washed in serum-free medium, counted and re-suspended in 1x PBS. 4 (Protocol A) or 16 (Protocol B) weeks old C57BL/6J *Gadd45b*$^{-/-}$ and *Gadd45b*$^{+/+}$ male recipients, carrying *Ptprc*^{b} (*CD45.2/Ly5.2*) alleles, were lethally irradiated with a single dose of 9.5 Gy and, 24 hours later, intravenously injected via the tail vein with 5 x 10^6 BM donor cells, in order to generate all four possible chimaerism combinations. BM reconstitution with CD45.1/Ly5.1$^+$ donor cells was verified after adoptive transfer by FACS analysis of blood leukocytes.

DEN Treatment and HCC Induction

For the initiation-only model of HCC, 15 to 17 days old *Gadd45b*$^{-/-}$ and *Gadd45b*$^{+/+}$ males on a C57Bl/6Jx129/SvJ or C57Bl/6J background, as indicated, were injected intraperitoneally with a single dose of DEN (5 mg/kg and 20 mg/kg, respectively; Sigma-Aldrich). At the indicated endpoints, mice were sacrificed and their livers removed, photographed and separated into individual lobes. Externally visible tumours (≥0.5mm) were measured using a caliper and counted. Tumour areas were calculated using the formula: $\pi(\text{diameter 1} + \text{diameter 2})^2/4$ (34). For histological evaluations, liver tissue was fixed in 10% neutral buffered formalin solution and paraffin embedded. The remaining liver tissue was microdissected into tumour and non-tumour tissue and stored at -80°C for molecular evaluation.

For HCC induction in the tumour initiation-promotion model, mice were treated according to two distinct experimental setups, designated as Protocol A and Protocol B. As part of Protocol A, 4 weeks old C57BL/6J males (CD45.2/Ly5.2$^+$) were adoptively transferred with BM from CD45.1/Ly5.1$^+$ males, and, 4 weeks later, intravenously treated twice with of 200 µL of clodronate liposomes to deplete endogenous Kupffer cells. Clodronate liposomes, containing approximately 5 mg/mL

of clodronate, were prepared as previously described and were provided by N. Van Rooijen (ClodronateLiposomes.org) (35). 10 weeks after clodronate liposome administration, BM chimaeras were intraperitoneally injected with a single dose of DEN (100 mg/kg; Sigma-Aldrich) and, 4 weeks later, placed on treatment with 0.07% of the tumour promoter, phenobarbital (Sigma-Aldrich), in the drinking water until the experimental endpoint, according to an established tumour initiation-promotion protocol (33). As part of Protocol B, 4 weeks old C57BL/6J males (CD45.2/Ly5.2$^+$) were intraperitoneally injected with 75 mg/kg of DEN (Sigma-Aldrich) and, 4 weeks later, placed on treatment with 0.07% phenobarbital (Sigma-Aldrich) in the drinking water, as above, in order to induce HCC initiation and early promotion. After 8 weeks, mice were adoptively transferred with BM from congenic CD45.1/Ly5.1$^+$ males and, 4 weeks later, treated with 200 µL of clodronate liposomes, as above, to deplete Kupffer cells. At the indicated endpoints, mice were sacrificed, and their livers removed, photographed and separated into individual lobes. Externally visible tumours (≥0.5 mm) were counted. For histological evaluations, liver tissue was fixed and paraffin-embedded or embedded in Tissue-Tek OCT compound (Sakura Finetek) for frozen block preparation. BM-cell reconstitution and liver repopulation with donor-derived CD45.1/Ly5.1$^+$ Kupffer cells were confirmed in each group of BM chimaeras by FACS analysis of spleen and BM cells and immunofluorescence staining of frozen liver sections, respectively.

To validate the procedure for Kupffer cell depletion, a separate group of C57BL/6J mice was intravenously injected with a single dose of 200 µL of clodronate or PBS liposomes. At the indicated time points, mice were sacrificed, and their livers and spleens were removed, fixed and paraffin-embedded for immunohistological evaluation of macrophage depletion.

Tumour Allografts

For fibrosarcoma allografts, 6 to 8 weeks old C57BL/6J *Gadd45b*$^{-/-}$ and *Gadd45b*$^{+/+}$ males were subcutaneously injected in the right flank with 1.0 x 10^5 MCA-203 cells in 100 µL of sterile 1x PBS, using a 1-mL Leur-Lok™ Tip syringe (BD Biosciences) with a 25-guage needle. MCA-203 cells were harvested from exponentially growing cultures, washed once with serum-free medium and re-suspended in 1x PBS immediately before injection. Once tumours became palpable, tumour growth was monitored every other day using a vernier caliper. Tumour volumes were calculated using the formula: volume = $AxB^2/2$ (where A is the larger diameter, and B is the smaller diameter of the tumour) (24). 19 days after tumour cell injection, mice were sacrificed, and tumours were removed and embedded in Tissue-Tek OCT compound (Sakura Finetek) for frozen block preparation. To investigate the macrophage-specific role of Gadd45β in sarcomagenesis, 6 to 8 weeks old *Gadd45b*$^{F/F}$ and *Gadd45b*$^{\Delta/\Delta}$ males were injected with 1.0 x 10^5 exponentially growing MCA-203 cells in 200 µL of sterile 1x PBS containing Matrigel (1:1) (Corning). Tumour growth was monitored using a vernier caliper, and tumor volumes were calculated as above. At the indicated endpoint, mice were sacrificed, and tumours photographed.

For the *in vivo* depletion of $CD8^+$ T cells, 8 to 12 weeks old C57BL/6J *Gadd45b*$^{-/-}$ and *Gadd45b*$^{+/+}$ females mice were treated intraperitoneally with 250 µg of anti-CD8b antibody (Lyt 3.2; clone 53-5.8; BioXCell) or rat IgG isotype-matched control antibody (clone HRPN; BioXCell) at day -1 and day 0 before the injection of 1.0 x 10^5 exponentially growing MCA-203 cells prepared as described above, and then twice a week with the same dose of antibody until the experimental endpoint. Tumour growth was monitored as described above. The efficiency of the antibody-mediated $CD8^+$ T-cell depletion was determined by FACS analysis of spleen cells using anti-CD8b-APC (130-106-315), anti-CD4-APC (130-109-415) and anti-CD3-FITC (130-108-836) antibodies (Miltenyi Biotec).

For ovarian carcinoma allografts, 11 to 12 weeks old C57BL/6J *Gadd45b*$^{-/-}$ and *Gadd45b*$^{+/+}$ females were intraperitoneally injected with exponentially growing 1.0 x 10^6 ID8-Luc cells in 300 µL of sterile saline solution, using a 1-mL Leur-Lok™ Tip syringe (BD Biosciences) with a 25-guage needle. Tumour growth was monitored weekly starting 6 weeks after tumour cell injection by bioluminescence imaging.

The analyses of the macrophage-specific role of Gadd45β in ovarian oncogenesis were performed essentially as previously described (18). Briefly, 8 weeks old C57BL/6J *Gadd45b*$^{+/+}$ females (Harlan Laboratories) were intraperitoneally injected with 2 x 10^6 exponentially growing ID8-Luc cells in 300 µL of sterile saline solution, and tumours were allowed to grow, as above. After 5 weeks, mice were randomised into two groups and intraperitoneally injected with 10 x 10^6 BMDMs from C57BL/6J *Gadd45b*$^{-/-}$ or *Gadd45b*$^{+/+}$ mice in 300 µL of sterile saline solution. ID8-Luc tumour growth was monitored weekly by bioluminescence imaging. Further information on the procedures used for bioimaging can be found in the Supplementary Information.

Histopathological Analyses, Immunohistochemistry, Immunofluorescence and TUNEL Assays

Detailed information on the procedures used for histopathological analyses, immunohistochemistry, immunofluorescence and TUNEL assays can be found in the Supplementary Information.

Quantitative Real-Time Polymerase-Chain Reaction (qRT-PCR) Analysis, Western Blots and FACS Analysis

Detailed information on the procedures used for RNA extraction, qRT-PCR reactions, western blotting and FACS analysis can be found in the Supplementary Information.

Statistical Analysis

Data were analyzed using Graph Pad Prism version 7.0 (GraphPad Software) or R (www.R-project.org). Statistical analyses of the results were performed using either two-tailed t test or two-tailed Mann-Whitney U test, depending on the distribution of the data. Assumptions concerning the data (for example, normal distribution and similar variation between experimental groups) were examined for appropriateness before statistical tests were conducted. p values < 0.05 were considered statistically significant. For ovarian carcinoma allografts, outliers were detected and removed according to the default options of the software used.

Survival analyses were performed in R, using package survival. Differences between the survival distributions within each dataset were assessed for statistical significance using Kaplan-Meier curves and the log-rank test, with p values < 0.05 taken as the level of significance.

For the sample size of the animals used in this study, it was fixed in a prospective manner; no statistical method was used to predetermine sample size. Mice with the indicated genotypes were included in the study without any randomization. Histological analyses were performed in a single-blinded fashion. No blinding was used for the remaining analyses.

RESULTS

GADD45B Expression Denotes Aggressive Malignant Disease Across Most Human Cancers

We recently identified the product of the NF-κB-regulated gene, *GADD45B*, as an essential survival factor and novel therapeutic target in multiple myeloma (24). We therefore investigated whether *GADD45B* was involved in any types of malignancy beyond multiple myeloma. Strikingly, in publicly available patient datasets, elevated *GADD45B* expression correlated with rapid disease progression in thirteen out of the top fifteen solid cancers for mortality worldwide (36). When patients with prevalent disease subtypes were stratified at diagnosis on the basis of *GADD45B* expression in the tumour tissues, the patient cohorts expressing high *GADD45B* levels exhibited significantly shorter recurrence-free survival (RFS) and/or overall survival (OS) than the corresponding cohorts expressing low *GADD45B* mRNA levels (Figures 1A-1M). Collectively, these results identify GADD45β as a hallmark of aggressive pathology across the most prevalent human cancer types and postulate its general clinical significance in malignant disease.

Gadd45b Loss Reduces Chemically Induced Hepatocellular Carcinogenesis

The role of IKKβ/NF-κB in hepatocellular carcinogenesis is controversial (16,17). Indeed, in the widely used diethylnitrosamine (DEN) experimental model of HCC, hepatocyte-specific *Ikkb* ablation was previously shown to promote, rather than inhibit, oncogenesis (33). Therefore, to clarify the basis for the observed correlation between expression of the IKKβ/NF-κB-regulated effector, *GADD45B*, and aggressive disease pathology in HCC datasets (Figure 1C), we sought to investigate whether Gadd45β was involved in this process. 15-day-old *Gadd45b*$^{-/-}$ and

Gadd45b$^{+/+}$ C57BL/6 males were treated with a single intraperitoneal injection of the carcinogen, DEN, according to an established protocol for HCC induction (33). As expected, all *Gadd45b*$^{+/+}$ mice given DEN developed typical HCCs within 9 months (Figures 2A-2E). Interestingly, *Gadd45b* deletion significantly reduced the number of HCCs (Figure 2A, Figure 2D). Tumour surface area and maximum tumour diameter were also markedly reduced in *Gadd45b*$^{-/-}$ mice relative to controls (Figures 2B-2C).

Histological analysis confirmed the more than three-fold lower number of HCCs in *Gadd45b*$^{-/-}$ than *Gadd45b*$^{+/+}$ livers (Figure 2F). As typically seen in C57BL/6 mice, DEN-induced tumours predominantly consisted of adenomas, with only few sporadic carcinomas, hereafter collectively referred to as HCCs. Similar results were obtained using 129/SvJxC57BL/6 mice (Figures S1A-S1F). Notably, *Gadd45b*$^{-/-}$ and *Gadd45b*$^{+/+}$ HCCs displayed no difference with respect to tumour grade, mitotic index or necrosis grade, and similar percentages of proliferating and apoptotic cells (Figures S1G-S1J). Likewise, the analysis of cell-cycle regulators and oncogenic factors showed no difference between *Gadd45b*$^{-/-}$ and *Gadd45b*$^{+/+}$ livers when comparing corresponding tumour or non-tumour tissues (Figure S1K). Hence, opposite to hepatocyte-specific *Ikkb* loss (33), *Gadd45b* ablation inhibits DEN-induced hepatocellular carcinogenesis, while having no effect on tumour cell proliferation or apoptosis.

Gadd45b Loss Augments Tumour-Associated Macrophage and T-Cell Infiltration and TLS Formation

Despite the otherwise similar histological and molecular characteristics (Figure 2E, Figure S1E, Figures S1G-S1K), *Gadd45b*$^{-/-}$ HCCs contained considerably more and larger immunoinflammatory infiltrates than *Gadd45b*$^{+/+}$ tumours (Figure 2G; see also

Figure 2E, Figure 2H, Figure S1E). Strikingly, in *Gadd45b*$^{-/-}$, but not *Gadd45b*$^{+/+}$ HCCs, intratumoural infiltrates were also often organised into follicle-like aggregates, reminiscent of tertiary lymphoid structures (TLSs) (Figures 2G-2J; see also Figure 2E, Figure S1E, Figure S2A-S2B), denoting sites of thriving adaptive immune reactions and favourable clinical outcome in multiple human cancers (37). Consistently, whereas only 33% of *Gadd45b*$^{+/+}$ mice contained at least one HCC featuring TLS-like aggregates (hereafter referred to as TLSs), well-organised TLSs were often found in multiple HCCs in 80% of *Gadd45b*$^{-/-}$ mice (Figure S2C; see also Figure S2D).

In both *Gadd45b*$^{-/-}$ and *Gadd45b*$^{+/+}$ HCCs, intratumoural leukocyte infiltrates predominantly consisted of lymphocytes and macrophages, with only few sparse granulocytes (Figures 2I-2J). However, *Gadd45b*$^{-/-}$ HCCs contained considerably more F4/80^{+} and IBA-1^{+} macrophages and B and T lymphocytes than *Gadd45b*$^{+/+}$ HCCs (Figures 2I-2J; see also Figures 3A-3B). Crucially, *Gadd45b* loss also increased the intratumoural infiltration by CD8^{+} T cells, a hallmark of effective antitumour immune responses (Figures 2I-2J). Interestingly, whereas the increased numbers of IBA-1^{+} macrophages and lymphocytes observed in *Gadd45b*$^{-/-}$ HCCs were mostly due to the greater frequency and larger size of TLSs, the increased intratumoural F4/80^{+} macrophage numbers were mainly attributable to the higher density of these cells outside TLSs. Plausibly, this distinct effect of *Gadd45b* loss on the F4/80^{+} macrophage distribution within the TME reflects the central role of these cells in sensing “danger” signals and antigens arising from tumour cells and processing them into cues to elicit reciprocal adaptive immune reactions (38). Irrespective of the mechanism(s), our data demonstrate that *Gadd45b* loss profoundly affects tumour-associated inflammation and macrophage and lymphocyte infiltration within DEN-induced HCCs.

Since resident liver macrophages, so-called Kupffer cells, play a central role in DEN-induced carcinogenesis through a mechanism that depends on IKK/NF-κB (17,33), we further investigated the effect of Gadd45β on TAMs. In keeping with their heightened state of inflammation, *Gadd45b*$^{-/-}$ HCCs contained a significantly higher number of myeloid-like cells expressing inflammatory markers, such as inducible nitric-oxide synthase (iNOS) and cyclo-oxygenase-2 (COX-2), than *Gadd45b*$^{+/+}$ HCCs (14) (Figures 3A-3B, Figure S2E). They also contained markedly more IBA-1^{+} macrophages within well-organised TLSs expressing major histocompatibility complex class II (MHC-II), a key antigen-presenting molecule and prototypical proinflammatory activation marker (7) (Figures 3C-3D; see also Figures 3A-3B, Figure S2E), thus phenocopying the effects of myeloid-associated IKKβ/NF-κB inhibition on TAMs (18,19). Underscoring the significance of these findings, *Gadd45b*$^{-/-}$ HCCs additionally displayed considerably more TLS-associated cells expressing the immunoinhibitory enzyme, indoleamine-2,3-dioxygenase (IDO) (Figures 3E-3F), suggesting that the upregulation of immune checkpoint molecules, such as IDO (3,4), could conceal the full immunostimulatory potential of *Gadd45b* loss. By contrast, *Gadd45b* deletion had no effect on alternative TAM activation, which is more typical of established neoplasias (7,8) (Figures 3A-3B; see also Figure S2E). Hence, *Gadd45b* loss enhances proinflammatory TAM activation within HCCs. Collectively, these findings indicate that Gadd45β plays an essential role in curbing proinflammatory TAM activation, intratumoural lymphocyte infiltration and TLS formation within established neoplasias.

Gadd45b Loss Augments DEN-Induced Hepatocyte Toxicity, But Not Hepatocyte Proliferation

While in established tumours macrophage-driven inflammation has the potential to elicit antitumour immune responses, it was shown that when it ensues in response to acute DEN-induced liver damage, this inflammation triggers compensatory hepatocyte proliferation, thereby facilitating HCC initiation (33). We therefore examined the effect of *Gadd45b* loss on the acute liver response to DEN administration. As expected, in *Gadd45b*$^{+/+}$ mice, DEN injection induced hepatocyte apoptosis at 48 hr (Figures S3A-S3B). The number of apoptotic hepatocytes was modestly increased, in *Gadd45b*$^{-/-}$ mice after DEN administration, but not at baseline, compared to controls (Figures S3A-S3B). Circulating liver enzymes, indicative of hepatocyte damage, were also higher in DEN-treated *Gadd45b*$^{-/-}$ than *Gadd45b*$^{+/+}$ mice (Figure S3C), even though the livers of these mice displayed similarly low numbers of dead cells (Figures S3D-S3E).

Since DEN-induced hepatocyte toxicity involves JNK activation (33,39), and Gadd45β has the capacity to suppress JNK signalling in the liver (32), we investigated the effects of *Gadd45b* loss on MAPK activation by DEN. As shown in Figure S3F, DEN induced strong JNK activation in *Gadd45b*$^{+/+}$ livers, but this activation was unaffected by *Gadd45b* loss. *Gadd45b* deficiency also had no effect on DEN-induced ERK, p38 or STAT3 signalling, nor did it have any effect on hepatocyte proliferation, either at baseline or following DEN injection (Figures S3G-S3H). Hence, *Gadd45b* loss mildly augments DEN-induced liver damage, but does not affect hepatocyte proliferation and is, therefore, unlikely to impact HCC development by affecting the acute liver response to DEN.

Haematopoietic Cell-Specific *Gadd45b* Loss Reduces DEN-Induced Carcinogenesis

Given the association between diminished HCC burden and increased intratumoural immunoinflammatory infiltration observed in *Gadd45b*$^{-/-}$ mice, we hypothesised that Gadd45β promotes hepatocellular carcinogenesis by operating within immune and inflammatory cells. To distinguish between the oncogenic roles of Gadd45β in the TME and the hepatic parenchyma, we generated bone marrow (BM) chimaeras harbouring all possible combinations of tissue-specific *Gadd45b* deficiency in the parenchymal tissue and BM-derived cells (Figure 4A). Given the importance of Kupffer cells in driving DEN-induced carcinogenesis (17,33), chimaeric mice were then treated with clodronate liposomes to deplete endogenous Kupffer cells and thereby permit liver repopulation with donor-derived Kupffer cells, following which, mice were administered DEN, along with the tumour promoter, phenobarbital (Protocol A; Figure 4A), according to an established tumour initiation-promotion protocol (33).

Successful BM-cell reconstitution and host Kupffer-cell liver repopulation with donor-derived Kupffer cells were confirmed by FACS and immunofluorescence analyses, respectively (Figures S4A-S4B; see also Figure S4C). As expected, DEN-treated chimaeras bearing isogenic *Gadd45b*$^{+/+}$ or *Gadd45b*$^{-/-}$ tissues (WT_{BM}:WT_{Host} and KO_{BM}:KO_{Host}, respectively) developed similar numbers of HCCs as their non-transplanted counterparts (Figures 4B-4C; see also Figure 2A, Figure S1A). Notably, however, the ratio between HCC numbers in these mice was more than five folds (Figure 4B; compare WT_{BM}:WT_{Host} with KO_{BM}:KO_{Host}) relative to the approximately two-fold ratio observed in mice treated according to the tumour initiation-only protocol (Figure 2A, Figure S1A), suggesting that *Gadd45b* loss has a greater impact on HCC progression than on tumour initiation (discussed below).

Strikingly, selective *Gadd45b* ablation in BM-derived cells reduced the numbers of HCCs to similar levels as in isogenic *Gadd45b*$^{-/-}$ mice (Figure 4B; compare KO_{BM}:WT_{Host} with WT_{BM}:WT_{Host}; also compare KO_{BM}:WT_{Host} with

KO_{BM}:KO_{Host}). By contrast, selective *Gadd45b* deletion in the hepatic parenchyma did not significantly affect HCC burden (compare WT_{BM}:KO_{Host} with WT_{BM}:WT_{Host}). In keeping with these findings, the additional *Gadd45b* ablation in BM-derived cells did result in a significant reduction in tumour numbers in *Gadd45b*$^{-/-}$ hosts (compare WT_{BM}:KO_{Host} with KO_{BM}:KO_{Host}). Hence, selective *Gadd45b* loss in hematopoietic-derived cells is sufficient on its own to fully recapitulate the phenotype of *Gadd45b*$^{-/-}$ mice in DEN-induced carcinogenesis. We concluded that Gadd45β promotes this oncogenic process largely by operating within immune and inflammatory cells.

Gadd45b Loss Hinders HCC Progression

Given that the effect of *Gadd45b* loss on DEN-induced carcinogenesis intensifies in a tumour initiation-promotion model (Figures 4B-4C), is associated with increased TME-based inflammation (Figures 2G-2J, Figures 3A-3F, Figures S2A-S2E), and does not affect the acute hepatocyte proliferative response to DEN (Figures S3G-S3H), we hypothesised that Gadd45β contributes to HCC progression, rather than initiation. As part of so-called "Protocol B" (Figure 4D), mice of both genotypes were first challenged with DEN and placed on treatment with phenobarbital, and then adoptively transferred with *Gadd45b*$^{-/-}$ or *Gadd45b*$^{+/+}$ BM, followed by Kupffer cell depletion, as for Protocol A. Because, the *Gadd45b* status of inflammatory cells is modified 3 months after DEN injection, when preneoplastic foci have already largely progressed to HCCs (40), we reasoned that Protocol B would allow to distinguish between roles of Gadd45β in tumour progression versus roles in tumour initiation.

Successful BM-cell engraftment and Kupffer-cell liver repopulation with donor-derived cells were verified as for Protocol A (Figures S4D-S4E). As expected, 12 months after DEN injection, the ratio between HCC numbers of isogenic *Gadd45b*$^{+/+}$ and *Gadd45b*$^{-/-}$ mice was similar to that observed with Protocol A

(Figures 4E-4F; compare KO_{BM}:KO_{Host} with WT_{BM}:WT_{Host}; see also Figures 4B-4C). Strikingly, even when introduced after tumour initiation had already largely occurred in *Gadd45b*$^{+/+}$ livers, BM-derived cell-specific *Gadd45b* ablation retained a virtually intact capacity to diminish oncogenesis (Figure 4E; compare KO_{BM}:WT_{Host} with WT_{BM}:WT_{Host}). Accordingly, concomitant *Gadd45b* ablation in the hepatic parenchyma had no additional effect on HCC burden (compare KO_{BM}:WT_{Host} with KO_{BM}:KO_{Host}). Reciprocally, the introduction of *Gadd45b*$^{+/+}$ BM into *Gadd45b*$^{-/-}$ hosts, 3 months after DEN injection, was still effective in restoring oncogenesis (compare WT_{BM}:KO_{Host} with KO_{BM}:KO_{Host}). Notably, these results were broadly equivalent to those obtained with Protocol A (see Figure 4B). Collectively, these findings reinforce the conclusions that the Gadd45β oncogenic function in DEN-induced tumourigenesis is largely restricted to the haematopoietic system and impacts upon tumour progression, while likely having little impact upon tumour initiation.

TME-Associated *Gadd45b* Loss in Fibrosarcoma Augments TAM Infiltration and Proinflammatory Activation, While Reducing Tumour Growth

To clarify the basis for the tumour-promoting activity of Gadd45β in the TME and its significance in the association between *GADD45B* expression and aggressive disease pathology across human cancer types (Figures 1A-1M), we sought to investigate other model systems of established neoplasia, in which IKK/NF-κB drives oncogenesis by operating in immunoinflammatory cells. We reasoned that this approach could additionally clarify the basis for the oncogenic function of IKK/NF-κB itself in these cells. Indeed, while IKK/NF-κB inhibition in different epithelial cell types was shown to have discordant outcomes on oncogenesis, this inhibition in inflammatory cells, especially those of the myeloid lineage, has invariably resulted in

oncogenesis suppression (16). We chose an initiated fibrosarcoma model in which haematopoietic cell-specific NF-κB1/p105 ablation was shown to augment TME-based inflammation and proinflammatory TAM activation, resulting in diminished tumour growth (19). As expected, subcutaneously implanted MCA-203 fibrosarcomas grew rapidly in immunocompetent C57BL/6 *Gadd45b*$^{+/+}$ mice (Figure 5A). Notably, however, tumour growth was markedly reduced in *Gadd45b*$^{-/-}$ hosts, thereby confirming in a different model system the essential oncogenic role of Gadd45β in the TME.

As seen with HCC (Figures 2I-2J, Figures 3A-3D), the *Gadd45b*$^{-/-}$ TME contained a higher number of TAMs than the *Gadd45b*$^{+/+}$ TME (Figures 5B, Figure S5A). Fibrosarcomas from *Gadd45b*$^{-/-}$ mice also contained more T cells than tumours from *Gadd45b*$^{+/+}$ hosts, although at the early time point examined (*i.e.*, d19), this T-cell increase had not reached statistical significance (Figures 5B, Figure S5A). Plausibly, this reflected the rapid evolution of fibrosarcoma allografts relative to endogenous DEN-induced HCCs and the delayed onset of adaptive relative to innate immune reactions (see also Figures 2I-2J). Indeed, the depletion of cytotoxic CD8^{+} T cells by the use of a CD8-specific antibody resulted in a marked increase in fibrosarcoma growth, completely ablating any inhibitory effect of *Gadd45b* loss on oncogenesis (Figures 5C-5D, Figure S5B; compare tumour growth in *Gadd45b*$^{-/-}$ mice treated with anti-CD8 versus control antibody; also note the similar tumour growth in *Gadd45b*$^{-/-}$ and *Gadd45b*$^{+/+}$ mice treated with the anti-CD8 antibody; see also Figure S5C). These data unequivocally demonstrate the critical importance of cytotoxic CD8^{+} T cells in the antitumor effect of TME-associated *Gadd45B* loss. By contrast, TME-infiltrating B cells and granulocytes were unaffected by *Gadd45b* loss.

Underscoring the significance of the effects of Gadd45β on TAMs, these cells comprised the major cellular component of the immunoinflammatory infiltrate in the *Gadd45b*$^{-/-}$ TME. Strikingly, the *Gadd45b*$^{-/-}$ TME also contained an approximately

four-fold higher number of TAMs expressing the proinflammatory markers, iNOS and COX-2 (14), than the *Gadd45b*$^{+/+}$ TME (Figures 5E, Figure S5D). Reciprocally, fibrosarcomas from *Gadd45b*$^{-/-}$ mice displayed a lower number of Ym-1/Chi3l3^{+} TAMs than tumours from *Gadd45b*$^{+/+}$ mice. Other antiinflammatory activation markers were instead unaffected by *Gadd45b* loss (14). Hence, TME-associated *Gadd45b* ablation augments TAM infiltration, proinflammatory TAM activation and CD8^{+} T cell-driven antitumor immune responses in fibrosarcoma, thus reinforcing our findings with DEN-induced HCC.

TME-Specific *Gadd45b* Loss Augments Proinflammatory TAM Activation and Intratumoural T-Cell Infiltration, While Reducing Ovarian Oncogenesis

To further understand the general significance of Gadd45β in TAM activation and malignant progression, we examined a third cancer model in which IKK/NF-κB was shown to drive oncogenesis by operating in myelo-monocytic cells. We used ID8-Luc ovarian adenocarcinoma allografts because previous studies had shown that macrophage-specific IKKβ inhibition in this model reverses the typical antiinflammatory TAM phenotype and enhances proinflammatory TAM activation, thereby causing tumour regression (18). Consistently, whereas syngeneic ID8-Luc tumours grew rapidly in the peritoneum of *Gadd45b*$^{+/+}$ mice, tumour growth was markedly reduced in *Gadd45b*$^{-/-}$ mice (Figures 5F-5G), thus demonstrating that TME-specific *Gadd45b* ablation also curbs ovarian oncogenesis.

Notably, intratumoural leukocyte infiltrates yielded a higher number of TAMs, T cells and granulocytes, but not B cells, in *Gadd45b*$^{-/-}$ compared to *Gadd45b*$^{+/+}$ mice (Figure 5H). Significantly, as seen in DEN-induced HCC (Figures 2I-2J), the relative

T-cell abundance in the *Gadd45b*$^{-/-}$ TME was largely due to an increased influx of CD8^{+} cytotoxic T cells, which drive effective antitumour immune reactions (3,5) (Figure 5H), rather than CD4^{+} T cells. Consistent with the increased immunoreactivity of the *Gadd45b*$^{-/-}$ TME, a larger proportion of *Gadd45b*$^{-/-}$ than *Gadd45b*$^{+/+}$ TAMs expressed high surface levels of MHC-II (Figures 5I-5J, Figure S5E). Purified *Gadd45b*$^{-/-}$ TAMs also expressed higher levels of other proinflammatory genes, including *Nos2*, *Cxcl9*, *Cxcl10*, *Tnfa* and *Il-6*, than *Gadd45b*$^{+/+}$ TAMs, whereas antiinflammatory activation genes, with the exception of *Ym-1/Chi3l3*, were unaffected by *Gadd45b* loss (14) (Figure 5K, Figure S5F). In keeping with their heightened state of immune activation, *Gadd45b*$^{-/-}$ TAMs additionally expressed higher levels of immune checkpoint molecule-encoding genes, *e.g.*, *Ido*, *Ctla-4*, *Pd-l1*, and *B7-h3* (3,4) (Figure 5L), thus confirming the observations made with DEN-induced HCC (Figures 3E-3F). Hence, in three distinct models of solid cancer, TME-specific *Gadd45b* ablation increased proinflammatory TAM activation, and intratumoural macrophage and CD8^{+} T-cell infiltration (see also Figures 2G-2J, Figures 3A-3F, Figure 5B, Figure 5E, Figures 5H-5L, Figure S2E, Figure S5A, Figures S5D-S5E), resulting in diminished tumour growth. Interestingly, these effects of *Gadd45b* loss on oncogenesis phenocopied the effects of myeloid-specific IKKβ/NF-κB inhibition (16,18,19). Collectively, these findings underpin the importance of the TME-specific role of Gadd45β in curbing tumour-associated inflammation and immune infiltration across different cancer types.

Gadd45b Loss Promotes Proinflammatory Macrophage Activation via a Cell-Autonomous Mechanism

We sought to investigate whether Gadd45β mediated its effects on TAM activation via a cell-autonomous mechanism. We used an *ex-vivo* co-culture model system

mimicking the tumour-cell/macrophage interactions occuring in cancer, *in vivo* (18). Consistent with our *in-vivo* findings (Figures 5E, Figure S5D), upon co-culture with MCA-203 cells, *Gadd45b*$^{-/-}$ BM-derived macrophages (BMDMs) expressed markedly higher levels of proinflammatory M1-like genes, including *Nos2*, *Tnfa* and *Cxcl10*, and lower levels of *Arg-1*, but not of other antiinflammatory M2-like genes, than *Gadd45b*$^{+/+}$ BMDMs (Figure 6A). Similar results were obtained when *Gadd45b*$^{-/-}$ and *Gadd45b*$^{+/+}$ BMDMs were co-cultured under similar conditions with ID8-Luc carcinoma cells (Figure S6A; see also Figures 5I-5K, Figure S5F). Hence, Gadd45β plays an essential and cell-autonomous role in restraining proinflammatory macrophage activation in response to cues from tumour cells.

To clarify the mechanisms by which Gadd45β governs tumour cell-induced macrophage activation, we used a tumour cell-free model system, which employs cytokines and TLR ligands to polarise macrophages (7,8). As expected, proinflammatory M1-like genes, as well as known NF-κB target genes, including *Gadd45b*, *Nfkbia* and *Tnfaip3*, were strongly upregulated by IFN-γ and lipopolysaccharide (LPS) in *Gadd45b*$^{+/+}$ BMDMs (Figure 6B). Each of the proinflammatory M1-like genes tested, however, was further significantly upregulated in IFN-γ/LPS-treated *Gadd45b*$^{-/-}$ BMDMs compared to *Gadd45b*$^{+/+}$ BMDMs. Immune checkpoint molecule-coding genes, including *Ido* and *Pd-l2*, were also markedly increased in IFN-γ/LPS-stimulated *Gadd45b*$^{-/-}$ BMDMs relative to controls (Figure 6B), in keeping with our *in vivo* findings (Figures 3E-3F, Figure 5L). By contrast, *Gadd45b* expression was unaffected by treatment with IL-4 and IL-13, as was the upregulation of each of the antiinflammatory M2-like genes analysed (Figure 6C). We concluded that Gadd45β is required to curb inflammation and M1-like macrophage activation, but is not directly involved in antiinflammatory M2-like polarisation, suggesting that the perturbation of the antiinflammatory activation profile of *Gadd45b*$^{-/-}$ TAMs, occasionally observed in co-culture systems and *in vivo*,

stemmed from the skewing of these cells toward a proinflammatory activation phenotype. Collectively, these findings provide a mechanism for the effect of *Gadd45b* loss on tumour-associated inflammation and proinflammatory TAM polarisation, *in vivo*.

Gadd45b Loss Exacerbates Proinflammatory M1-Like Polarisation by Enhancing p38 Signalling

To further the mechanistic understanding of the role of Gadd45β in macrophage polarisation, we examined STAT1 and MAPK signalling, which upregulates the M1-like activation programme downstream of IFN-γ receptor (IFN-γR) and TLRs (41). As shown in Figures 6D-6E, stimulation with IFN-γ and LPS activated these pathways, as well as Gadd45β expression, in *Gadd45b*$^{+/+}$ BMDMs. Yet, *Gadd45b* deletion had no effect on either STAT1 or ERK phosphorylation, nor did it have any effect on JNK signalling, nor on NF-κB activation (Figures 6D-6E). Surprisingly, *Gadd45b* loss instead markedly augmented and prolonged IFN-γ/LPS-induced p38 signalling, at each of the time points examined (Figure 6D). We concluded that Gadd45β is required to restrict both the magnitude and duration of p38 activation during proinflammatory macrophage polarisation.

Since p38 governs inflammation and expression of many of the proinflammatory M1-denoting genes deregulated by *Gadd45b* loss (42), we hypothesised that Gadd45β inhibits proinflammatory macrophage polarisation by restraining exacerbated p38 signalling. We therefore investigated whether attenuating this signalling reversed the effects of *Gadd45b* loss on macrophage activation. Notably, treatment with the specific p38α/β inhibitor, Vx745 (http://www.kinase-screen.mrc.ac.uk/screening-compounds/348786), downregulated the IFN-γ/LPS-dependent induction of each of the proinflammatory M1-like genes

that were over-activated by *Gadd45b* loss to levels similar to those observed in IFN-γ/LPS-stimulated *Gadd45b*$^{+/+}$ BMDMs (Figure 6F; see also Figure 6B). Comparable results were obtained using two additional, structurally unrelated p38 inhibitors, *i.e.*, skepinone-L and SB203580, thus excluding any off-target effect of Vx745 (Figures S6B-S6C). We concluded that Gadd45β suppresses proinflammatory macrophage activation by selectively downregulating IFN-γ/LPS-induced p38 signalling.

Macrophage-Specific *Gadd45b* Loss Is Sufficient to Diminish Oncogenesis

To clarify the cause-effect relationship between macrophage-specific *Gadd45b* deficiency and oncogenesis suppression, we generated mice carrying homozygous loxP-flanked *Gadd45b* alleles (*Gadd45b*$^{F/F}$ mice; Figure 7A, Figures S7A-S7B), and crossed them with *LysM-cre* transgenic mice to obtain myeloid-specific Gadd45b null mice (*Gadd45b*$^{\Delta M/\Delta M}$), after Cre-mediated recombination (33) (Figure S7C). PCR analyses confirmed the selective excision of the *Gadd45b*^{F} alleles and the resulting ablation of *Gadd45b* mRNA expression in *Gadd45b*$^{\Delta M/\Delta M}$ splenic macrophages, but not splenic B or T lymphocytes (Figures 7B-7C).

Given that the *LysM-cre* transgene, which efficiently deletes loxP-targeted alleles in circulating myelo-monocytic cells, is not useful in Kupffer cells (33), *Gadd45b*$^{\Delta M/\Delta M}$ mice could not be tested in the DEN HCC model. We therefore used them in the context of MCA-203 fibrosarcoma allografts. As expected, MCA-203 tumour growth was unaffected by the presence of *Gadd45b*$^{F/F}$ alleles (Figures 7D-7E; see also Figure 5A). Strikingly, however, this growth was markedly diminished in *Gadd45b*$^{\Delta M/\Delta M}$ mice to a similar extent as seen in *Gadd45b*$^{-/-}$ mice (Figures 7D-7E; see Figure 5A), indicating that macrophage-specific *Gadd45b* loss is sufficient on its

own to fully recapitulate the effect of complete TME-based *Gadd45b* deficiency on inflammation-driven oncogenesis.

We sought to confirm this macrophage-specific role of Gadd45β in oncogenesis by using an alternative mouse model. To this end, ID8-Luc ovarian tumours were allowed to grow in *Gadd45b*$^{+/+}$ mice until they became detectable by bioimaging, at which point, mice were adoptively transferred with *ex-vivo* cultured *Gadd45b*$^{+/+}$ or *Gadd45b*$^{-/-}$ BMDMs (0 weeks; Figures 7F-7H). As expected, following *Gadd45b*$^{+/+}$ BMDM transfer, ovarian tumours continued to grow rapidly (Figures 7G-7H). By contrast, the transfer of *Gadd45b*$^{-/-}$ BMDMs resulted in a significant inhibition of tumour growth. As seen with fibrosarcoma (Figures 7D-7E), the effects of macrophage-specific *Gadd45b* loss on ovarian carcinogenesis recapitulated the tumour suppressive effect of complete TME-based *Gadd45b* ablation (Figures 5F-5G). Together with our findings with *Gadd45b*$^{\Delta M/\Delta M}$ mice, these results demonstrate that Gadd45β orchestrates the tumour-promoting activity of the TME across multiple cancer types by operating in myeloid cells. Collectively, our findings provide a mechanism for the immunosuppressive activity of the TME that restricts tumour-based inflammation and CD8$^+$ T-cell trafficking into tumours and underscore the general significance of the NF-κB-dependent mechanisms mediated by GADD45β in human malignant disease.

DISCUSSION

We have identified an essential innate immunity “checkpoint” governed by the GADD45β-dependent axis of the NF-κB pathway that counters TME-based inflammation and CD8$^+$ T-cell trafficking into tumours, the major barrier to effective anticancer immunotherapy (3,5). In three distinct models of cancers that are largely refractory to immunotherapies (43-45), myeloid-associated *Gadd45b* ablation

restored proinflammatory TAM activation and intratumoural $CD8^+$ T-cell infiltration, leading to diminished tumour growth. These findings uncover a mechanism for the immunusuppressive activity of the TME that fosters oncogenesis. They also provide a basis for the antiinflammatory role that IKKβ/NF-κB plays in the myeloid lineage and identify a candidate therapeutic route in the innate immune system for "re-educating" TAMs to overcome TME-mediated immunosuppression and, potentially, resistance to immunotherapies.

The treatment of certain malignancies is being revolutionised by the development of effective immunotherapies, such as antagonists of immune checkpoint molecules (4). Yet, the large majority of patients fails to respond to these treatments, due to the presence of additional immunoinhibitory mechanisms in the TME that prevent T-cell access into tumours or cause T-cell exhaustion (3,5). However, the limited understanding of these mechanisms, currently precludes the development of effective treatment strategies for breaking the TME-mediated resistance to immunotherapies. An attractive approach to overcome this resistance would be to harness the innate immune system to induce tumour-based inflammation and $CD8^+$ T-cell entry and expansion in the TME. Together, the myeloid-specific role of IKKβ/NF-κB in suppressing proinflammatory TAM activation (15) and the central role of myeloid cells in cancer immune evasion (6,7) provide a compelling rationale for therapeutically targeting IKKβ/NF-κB signalling to reprogramme TAMs toward a proinflammatory activation phenotype capable of eliciting local antitumour immune responses (18,19). Yet, no specific IKKβ/NF-κB inhibitor has so far been clinically approved.

Our finding that GADD45β mediates an essential innate immunoinhibitory mechanism therefore provides an attractive route downstream in the IKKβ/NF-κB pathway to redirect $CD8^+$ T-cell trafficking into tumours and reactivate silenced $CD8^+$ T-cell-driven antitumour immune responses. Congruently, in various cancer types,

selective Gadd45β ablation in myelo-monocytic cells closely phenocopied the effects of IKKβ/NF-κB inactivation on oncogenesis (15,16,18,19). Importantly, myeloid-specific Gadd45β deletion appeared to override TME-mediated $CD8^+$ T-cell exclusion, plausibly through a mechanism involving the upregulation of CXCR3-binding chemokines, *e.g.*, CXCL9, CXCL10 and CXCL11, which recruit Th-1-type and $CD8^+$ effector T cells into tumours and extranodal sites of inflammation (5,46). Underscoring the importance of the GADD45β-mediated function, the depletion of $CD8^+$ T cells completed abrogated any effect of myelod-restricted *Gadd45b* loss on oncogenesis. Indeed, Gadd45β blockade appeared to also enhance the ability of the TME to support T-cell effector functions by upregulating multiple inflammatory mediators, proinflammatory TAM functionalities and MHC-II molecules. Underscoring the coordinated nature of its multiple effects on the immune system, Gadd45β ablation further imparted anatomical organisation to adaptive immune reactions, enabling them to assemble into well-configured TLSs within endogenously arisen tumours.

Although Pikarsky and colleagues recently suggested that TLSs facilitate HCC initiation and early promotion, their study investigated TLS formation in the context of the preneoplastic hepatic parenchyma and inflamed neoplastic liver outside HCCs (47). Indeed, T- and B-cell immunity has been previously shown to counter DEN-induced HCC development in mouse models (47,48), and intratumoural TLSs have been shown to portend a favourable clinical outcome in the majority of human cancers, including HCC (37,49). Future studies will determine the precise mechanisms by which GADD45β curbs TME-based TLS formation and cytotoxic $CD8^+$ T-cell trafficking and activation, as well as how these mechanisms relate to the GADD45β-mediated antiinflammatory function in myeloid cells. Irrespective of the mechanisms, the profound effects of *Gadd45b* loss on macrophage and T-cell accumulation in the TME and intratumoural TLS formation underscore the broad

clinical potential of the GADD45β-dependent antiinflammatory axis of the IKK/NF-κB pathway in anticancer immunotherapy.

Since GADD45β also serves as an essential NF-κB-regulated inhibitor of cancer cell apoptosis (24), our finding of its unexpected function in the innate immune system demonstrates that a single pivotal axis of the IKK/NF-κB pathway, *i.e.*, the GADD45β-dependent axis, integrates the oncogenic mechanism suppressing tumour-cell apoptosis with the mechanism restraining TME-based inflammation and T-cell infiltration. Hence, GADD45β serves as a central downstream hub in the IKK/NF-κB pathway linking cancer and inflammation. Surprisingly, GADD45β appears to perform these oncogenic functions via separable, tissue-specific mechanisms, attenuating proinflammatory p38 signalling within TAMs to restrain proinflammatory activation, while inhibiting apoptosis of cancer cells by suppressing JNK/MKK7 signalling (24) (Figure 7I). Future studies will clarify the precise mechanism(s) by which GADD45β curbs p38 activation in myeloid cells and confirm the role of this mechanism in oncogenesis. Irrespective of these mechanism(s), our results postulate that targeting the IKKβ/NF-κB pathway through GADD45β inhibition provides a candidate therapeutic route to counter oncogenesis by reversing TME-mediated immunosuppression and, at the same time, inducing apoptosis of cancer cells, thereby affording dual clinical benefit. Indeed, a combination of oncogenic mechanisms mediated by GADD45β in malignant and TME-based myeloid cells likely underpins the correlations between elevated *GADD45B* expression and poor clinical outcome observed in the large majority of human cancers.

To circumvent the limitations of IKK/NF-κB-targeting agents, we recently adopted the strategy of therapeutically targeting a non-redundant, pathogenically critical axis of the NF-κB pathway – similarly mediated by GADD45β – in multiple myeloma, rather than NF-κB globally (24,50). Initial results from the first-in-human

clinical study of GADD45β/MKK7-targeting therapeutics in patients with multiple myeloma preliminarily indicate the clinical safety of these agents, alongside cancer-selective pharmacodynamic response (L.T. and G.F., unpublished observations). These encouraging early clinical results suggest that it may be possible to similarly target the GADD45β-binding factor regulating p38 signalling in myeloid cells, in order to elicit antitumour inflammation. Notably, by converting tumours lacking a spontaneous $CD8^+$ T-cell infiltrate into $CD8^+$ T-cell-infiltrated tumours and, concurrently, upregulating immune checkpoint molecules, *e.g.*, IDO and PD-1 ligands, innate immunotherapies targeting GADD45β could conceivably overcome primary resistance to adaptive immunotherapies, and thereby increase response rates in currently recalcitrant cancer patient subsets (3,5).

Further studies will clarify the clinical benefit of combining GADD45β inhibitors with conventional immunotherapies. Notwithstanding, the remarkable consistency of the effects of meyloid-specific *Gadd45b* deletion on oncogenesis and the widespread correlation of *GADD45B* expression with aggressive disease pathology across most human cancer types underscore the general clinical significance of the GADD45β-mediated mechanism and, consequently, the potential of GADD45β-targeting therapeutics in human malignant disease. The new added focus provided by our current findings of a role of GADD45β in innate immune regulation will also invigorate the drug discovery effort to develop novel GADD45β-targeting immunotherapeutics for safely and effectively treating oncological diseases.

ACKNOWLEDGEMENTS

We thank N. van Rooijen for providing clodronate liposomes, I. Marigo and V. Bronte for providing the MCA-203 cell line, and J. Dyson for assistance with animal studies. We also thank V. Tybulewicz, A. Leonardi, G. Melino and J. Behmoaras for critical

reading of the manuscript. The work was supported in part by Cancer Research UK programme grant A15115, Medical Research Council (MRC) Biomedical Catalyst grant MR/L005069/1 and Bloodwise project grant 15003 to G.F., the Associazione Italiana per la Ricerca sul Cancro (AIRC) grants 1432 and 5172 and MIUR PRIN grant n° 2009EWAW4M_003 to F.Z., MIUR FIRB grant n° RBAP10A9H9 to E.A, and the Associazione Italiana per la Ricerca sul Cancro (AIRC) grant 15585 to A.S.. D.Ver. and B.D.F. were supported by the L'Aquila University Ph.D. program in Experimental Medicine, M.F. and D.Vec. were supported by the L'Aquila University Ph.D program in Biotechnology.

REFERENCES

1. Hanahan D, Weinberg RA. Hallmarks of cancer: the next generation. *Cell* **2011**;144, 646-674.
2. Grivennikov SI, Greten FR, Karin M. Immunity, inflammation, and cancer. *Cell* **2010**;140, 883-899.
3. Joyce JA, Fearon DT. T cell exclusion, immune privilege, and the tumor microenvironment. *Science* **2015**;348, 74-80.
4. Topalian SL, Drake CG, Pardoll DM. Immune checkpoint blockade: a common denominator approach to cancer therapy. *Cancer Cell* **2015**;27, 450-461.
5. Gajewski TF, Schreiber H, Fu YX. Innate and adaptive immune cells in the tumor microenvironment. *Nat. Immunol.* **2013**;14, 1014-1022.
6. Noy R, Pollard JW. Tumor-associated macrophages: from mechanisms to therapy. *Immunity* **2014**;41, 49-61.

7. Biswas SK, Allavena P, Mantovani A. Tumor-associated macrophages: functional diversity, clinical significance, and open questions. *Semin. Immunopathol*. **2013**;35, 585-600.
8. Qian BZ, Pollard JW. Macrophage diversity enhances tumor progression and metastasis. *Cell* **2010**;141, 39-51.
9. Ries CH, Cannarile MA, Hoves S, Benz J, Wartha K, Runza V, *et al*. Targeting tumor-associated macrophages with anti-CSF-1R antibody reveals a strategy for cancer therapy. *Cancer Cell* **2014**;25, 846-859.
10. Zhu Y, Knolhoff BL, Meyer MA, Nywening TM, West BL, Luo J, *et al*. CSF1/CSF1R blockade reprograms tumor-infiltrating macrophages and improves response to T-cell checkpoint immunotherapy in pancreatic cancer models. *Cancer Res*. **2014**;74, 5057-5069.
11. Strachan DC, Ruffell B, Oei Y, Bissell MJ, Coussens LM, Daniel D. CSF1R inhibition delays cervical and mammary tumor growth in murine models by attenuating the turnover of tumor-associated macrophages and enhancing infiltration by CD8+ T cells. *Oncoimmunology* **2013**;2(12):e26968.
12. Mitchem JB, Brennan DJ, Knolhoff BL, Belt BA, Zhu Y, Sanford DE, *et al*. Targeting tumor-infiltrating macrophages decreases tumor-initiating cells, relieves immunosuppression, and improves chemotherapeutic responses. *Cancer Res*. **2013**;73(3):1128-41.
13. DeNardo DG, Brennan DJ, Rexhepaj E, Ruffell B, Shiao SL, Madden SF, *et al*. Leukocyte complexity predicts breast cancer survival and functionally regulates response to chemotherapy. *Cancer Discov*. **2011**;1, 54-67.
14. Sica A, Mantovani A. Macrophage plasticity and polarization: in vivo veritas. *J. Clin. Invest*. **2012**;122, 787-795.
15. Lawrence T. Macrophages and NF-κB in cancer. *Current Topics Microbiology* **2011**;349, 171-184.

16. Ben-Neriah Y, Karin M. Inflammation meets cancer, with NF-κB as the matchmaker. *Nat. Immunol*. **2011**;12, 715-723.
17. DiDonato JA, Mercurio F, Karin M. NF-κB and the link between inflammation and cancer. *Immunol. Rev.* **2012**;246, 379-400.
18. Hagemann T, Lawrence T, McNeish I, Charles KA, Kulbe H, Thompson RG, *et al*. "Re-educating" tumor-associated macrophages by targeting NF-κB. *J. Exp. Med*. **2008**;205, 1261-1268.
19. Saccani A, Schioppa T, Porta C, Biswas SK, Nebuloni M, Vago L, *et al*. p50 nuclear factor-kappaB overexpression in tumor-associated macrophages inhibits M1 inflammatory responses and antitumor resistance. *Cancer Res*. **2006**;66, 11432-11440.
20. Lawrence T, Fong C. The resolution of inflammation: anti-inflammatory roles for NF-kappaB. *Int. J. Biochem. Cell Biol*. **2010**;42, 519-523.
21. Lawrence T, Bebien M, Liu GY, Nizet V, Karin M. IKKalpha limits macrophage NF-kappaB activation and contributes to the resolution of inflammation. *Nature* **2005**;434, 1138-1143.
22. Papa S, Zazzeroni F, Bubici C, Jayawardena S, Alvarez K, Matsuda S, *et al*. Gadd45 beta mediates the NF-kappa B suppression of JNK signalling by targeting MKK7/JNKK2. *Nat. Cell Biol.* **2004**;6, 146-153.
23. De Smaele E, Zazzeroni F, Papa S, Nguyen DU, Jin R, Jones J, *et al*. Induction of gadd45beta by NF-kappaB downregulates pro-apoptotic JNK signalling. *Nature* **2001**;414, 308-13.
24. Tornatore L, Sandomenico A, Raimondo D, Low C, Rocci A, Tralau-Stewart C, *et al*. Cancer-selective targeting of the NF-κB survival pathway with GADD45β/MKK7 inhibitors. *Cancer Cell* **2014**:26, 495-508.
25. Tomczak K, Czerwinska P, Wiznerowicz M. The Cancer Genome Atlas (TCGA): an immeasurable source of knowledge. *Contemp. Oncol. (Pozn).* **2015**;19, A68-A77.

26. Goldman M, Craft B, Swatloski T, Cline M, Morozova O, Diekhans M, *et al*. The UCSC Cancer Genomics Browser: update 2015. *Nucleic Acids Res.* **2015**;43(Database issue):D812-7 (2015).
27. Marisa L, de Reynies A, Duval A, Selves J, Gaub MP, Vescovo L, *et al*. Gene expression classification of colon cancer into molecular subtypes: characterization, validation, and prognostic value. *PLoS Med*. **2013**;10(5):e1001453.
28. Kim WJ, Kim EJ, Kim SK, Kim YJ, Ha YS, Jeong P, *et al*. Predictive value of progression-related gene classifier in primary non-muscle invasive bladder cancer. *Mol. Cancer* **2010**;9:3.
29. Tothill RW, Tinker AV, George J, Brown R, Fox SB, Lade S, *et al*. Novel molecular subtypes of serous and endometrioid ovarian cancer linked to clinical outcome. *Clin. Cancer Res.* **2008**;14(16), 5198-208.
30. Curtis C, Shah SP, Chin SF, Turashvili G, Rueda OM, Dunning MJ, *et al*. The genomic and transcriptomic architecture of 2,000 breast tumours reveals novel subgroups. *Nature* **2012**;486(7403), 346-52.
31. Hagemann T, Robinson SC, Schulz M, Trümper L, Balkwill FR, Binder C, *et al*. Enhanced invasiveness of breast cancer cell lines upon co-cultivation with macrophages is due to TNF-alpha dependent up-regulation of matrix metalloproteases. *Carcinogenesis* **2004**;25(8), 1543-9.
32. Papa S, Zazzeroni F, Fu YX, Bubici C, Alvarez K, Dean K, *et al*. Gadd45beta promotes hepatocyte survival during liver regeneration in mice by modulating JNK signaling. *J. Clin. Invest*. **2008**;118(5),1911-23.
33. Maeda S, Kamata H, Luo JL, Leffert H, Karin M. IKKβ couples hepatocyte death to cytokine-driven compensatory proliferation that promotes chemical hepatocarcinogenesis. *Cell* **2005**;121, 977-990.
34. Darani HY, Shirzad H, Mansoori F, Zabardast N, Mahmoodzadeh M. Effects of Toxoplasma gondii and Toxocara canis antigens on WEHI-164

fibrosarcoma growth in a mouse model. *Korean J. Parasitol.* **2009**;47(2), 175-7.

35. Van Rooijen N, Sanders A. Kupffer cell depletion by liposome-delivered drugs: comparative activity of intracellular clodronate, propamidine, and ethylenediaminetetraacetic acid. *Hepatology* **1996**;23, 1239-1243.
36. Global Burden of Disease Cancer Collaboration. The Global Burden of Cancer 2013. *JAMA Oncol.* **2015**;1, 505-527.
37. Dieu-Nosjean MC, Goc J, Giraldo NA, Sautès-Fridman C, Fridman WH. Tertiary lymphoid structures in cancer and beyond. *Trends Immunol*. **2014**;35, 571-580.
38. Ley K, Pramod AB, Croft M, Ravichandran KS, Ting JP. How Mouse Macrophages Sense What Is Going On. *Front. Immunol.* **2016**;7, 204.
39. Sakurai T, Maeda S, Chang L, Karin M. Loss of hepatic NF-kappa B activity enhances chemical hepatocarcinogenesis through sustained c-Jun N-terminal kinase 1 activation. *Proc. Natl. Acad. Sci. U S A*. **2006**;103, 10544-10551.
40. He G, Yu GY, Temkin V, Ogata H, Kuntzen C, Sakurai T, *et al*. Hepatocyte IKKbeta/NF-kappaB inhibits tumor promotion and progression by preventing oxidative stress-driven STAT3 activation. *Cancer Cell* **2010**;17, 286-297.
41. Arthur JS, Ley SC. Mitogen-activated protein kinases in innate immunity. *Nat. Rev. Immunol*. **2013**;13, 679-692.
42. Yang Y, Kim SC, Yu T, Yi YS, Rhee MH, Sung GH, *et al*. Functional roles of p38 mitogen-activated protein kinase in macrophage-mediated inflammatory responses. *Mediators Inflamm*. **2014**;2014:352371.
43. Gaillard SL, Secord AA, Monk B. The role of immune checkpoint inhibition in the treatment of ovarian cancer. *Gynecol. Oncol. Res. Pract*. **2016**;3,11.
44. Harding JJ, El Dika, Abou-Alfa GK. Immunotherapy in hepatocellular carcinoma: Primed to make a difference? *Cancer* **2016**;122, 367-377.

45. Roberts SS, Chou AJ, Cheung NK. Immunotherapy of Childhood Sarcomas. *Front. Oncol*. **2016**;5, 181.
46. Fearon DT. Immune-Suppressing Cellular Elements of the Tumor Microenvironment. *Annu. Rev. of Cancer Biol*. **2016**;1, 13.1-13.15.
47. Finkin S, Yuan D, Stein I, Taniguchi K, Weber A, Unger K, *et al*. Ectopic lymphoid structures function as microniches for tumor progenitor cells in hepatocellular carcinoma. *Nat. Immunol*. **2015**;16, 1235-1244.
48. Schneider C, Teufel A, Yevsa T, Staib F, Hohmeyer A, Walenda G, *et al*. Adaptive immunity suppresses formation and progression of diethylnitrosamine-induced liver cancer. *Gut*. **2012**;61, 1733-1743.
49. Wada Y, Nakashima O, Kutami R, Yamamoto O, Kojiro M. Clinicopathological study on hepatocellular carcinoma with lymphocytic infiltration. *Hepatology* **1998**;27, 407-414.
50. Karin M. Whipping NF-κB to Submission via GADD45 and MKK7. *Cancer Cell* **2014**;26(4), 447-449.

FIGURE LEGENDS

Figure 1. The Widespread Correlation between Elevated *GADD45B* Expression and Poor Clinical Outcome across Human Cancer Types

(A-M) Relapse-free survival (RFS) and overall survival (OS) in patients with the indicated malignant pathologies, representing thirteen out of the top fifteen solid cancers for mortality worldwide and deposited in the following publicly available datasets: The Cancer Genome Atlas (TCGA) program (A, B, C, F, G, H, K, L and M); the French National Cartes d'Identité des Tumeurs (CIT) program (D); the Tumour

Banks in the UK and Canada (E); the Chungbuk National University Hospital (I); and the Australian Ovarian Cancer Study, Royal Brisbane Hospital, Westmead Hospital and Netherlands Cancer Institute (J). Patients in each series were stratified at diagnosis in two groups on the basis of the *GADD45B* mRNA expression in the tumour tissues, as shown. p values are indicated.

Figure 2. Reduced DEN-Induced HCC Development with Increased Intratumoural Immunoinflammatory Infiltrates and TLS Formation in *Gadd45b*$^{-/-}$ Mice

(A-C) Number of tumours (≥0.5 mm) (A), tumour surface area (B), and maximum tumour diameter (C) in livers of *Gadd45b*$^{+/+}$ (n=9) and *Gadd45b*$^{-/-}$ (n=12) C57BL/6J males 9 months after DEN injection (20 mg/kg). Values denote means ± SEM.
(D) Gross liver morphology in representative mice from (A-C). Arrowheads indicate tumours.
(E) Images of H&E staining showing the liver histology in representative mice from (A-C). Hatched lines (top) indicate tumour areas. Solid lines (top) denote the areas magnified in the bottom panels. The arrowhead (bottom, right) indicates a typical immunoinflammatory aggregate. Scales and magnifications are shown.
(F) Number of histologically confirmed HCCs per examined liver sections from individual mice in (A-C). Each symbol represents an individual mouse. Horizontal lines denote means.
(G and H) Percentages of HCCs (G) and combined HCCs and preneoplastic foci (H) containing TLSs in *Gadd45b*$^{+/+}$ (n=19) and *Gadd45b*$^{-/-}$ (n=26) 129/SvJxC57BL/6J males 11 months after DEN injection (5 mg/kg). Each symbol represents an individual mouse. Horizontal lines denote means.

(I) Immunohistochemical (IHC) analysis showing the percentage of positive area or number of positive cells per field at 400x, as stated, of the indicated immune cell populations in HCCs from (G). Values denote means ± SEM (IBA-1: *Gadd45b*$^{+/+}$, n=47; *Gadd45b*$^{-/-}$, n=34. CD8: *Gadd45b*$^{+/+}$, n=37; *Gadd45b*$^{-/-}$, n=33. All other markers: *Gadd45b*$^{+/+}$, 24≤n≤26; *Gadd45b*$^{-/-}$, n=26 or n=27).

(J) Images of H&E and IHC staining of representative tumour sections from (I). Scales and magnifications are shown.

(A-C and F-I) *, $p<0.05$; **, $p<0.01$; ***, $p<0.001$.

See also Figure S1 and Figure S2.

Figure 3. *Gadd45b* Loss Increases Macrophage Infiltration and Proinflammatory TAM Activation within HCCs

(A) IHC analysis showing the percentage of positive area or number of positive cells per field at 400x, as stated, for the indicated macrophage (F4/80, IBA-1) and proinflammatory and antiinflammatory activation markers in HCCs from Figures 2A-2C.

(B) Images of IHC staining of representative tumour sections from (A). Images of *Gadd45b*$^{-/-}$ HCCs are shown for non-organised immunoinflammatoty cell clusters (middle) and well-organised TLSs (right). Insets denote magnified areas at the top right corners.

(C) Immunofluorescence analysis showing the percentages of IBA-1^{+} macrophages expressing MHC-II per field at 400x in HCCs from Figures 2A-2C.

(D) Images of immunofluorescence staining of representative tumour sections from (C). Red, anti-IBA-1; green, anti-MHC-II; blue, DAPI.

(E) IHC analysis showing the percentage of IDO-positive area per field at 400x in *Gadd45b*$^{+/+}$ and *Gadd45b*$^{-/-}$ HCCs from (A).

(F) Images of IHC staining of representative tumour sections from (E).

(A, C and E) Values denote means ± SEM (*Gadd45b*$^{+/+}$, 14≤n≤30; *Gadd45b*$^{-/-}$, 12≤n≤15). *, p<0.05; **, p<0.01; ***, p<0.001.

(B, D and F) Scales and magnifications are shown.

See also Figure S2 and Figure S3.

Figure 4. Reduction of DEN-Induced HCC Development by *Gadd45b* Deletion in BM-Derived Cells

(A) Summary of the treatment schedule used for Protocol A.

(B) Numbers of tumours (≥0.5 mm) in livers of WT_{BM}:WT_{Host} (n=40), KO_{BM}:KO_{Host} (n=25), KO_{BM}:WT_{Host} (n=36) and WT_{BM}:KO_{Host} (n=35) BM chimaeras at the time shown in (A).

(C) Gross liver morphology in representative mice from (B).

(D) Summary of the treatment schedule used for Protocol B.

(E) Numbers of tumours (≥0.5 mm) in livers of WT_{BM}:WT_{Host} (n=24), KO_{BM}:KO_{Host} (n=23), KO_{BM}:WT_{Host} (n=24) and WT_{BM}:KO_{Host} (n=29) BM chimaeras at the time shown in (D).

(F) Gross liver morphology in representative mice from (E).

(A-F) WT, *Gadd45b*$^{+/+}$; KO, *Gadd45b*$^{-/-}$. BM chimaeras are identified as per "bone marrow donor:recipient" genotypes.

(B and E) Values denote means ± SEM. *, p<0.05; **, p<0.01; ***, p<0.001; ****, p<0.0001.

(C and F) Arrowheads denote tumours.

See also Figure S4.

Figure 5. Increased Intratumoural Immunoinflammatory Infiltration, Proinflammatory TAM Activation and Reduced Fibrosarcoma and Ovarian Carcinoma Growth in *Gadd45b*$^{-/-}$ mice

(A) Volumes of subcutaneous MCA-203 fibrosarcoma allografts in *Gadd45b*$^{+/+}$ (n=10) and *Gadd45b*$^{-/-}$ (n=9) mice at the times shown.

(B) IHC analysis showing the percentage of positive areas per field at 400x of the indicated immune cell populations in MCA-203 tumours from *Gadd45b*$^{+/+}$ (n=7) and *Gadd45b*$^{-/-}$ (n=8) mice 19 days after tumour cell injection.

(C) Volumes of subcutaneous MCA-203 fibrosarcoma allografts in *Gadd45b*$^{+/+}$ and *Gadd45b*$^{-/-}$ mice treated with anti-CD8 or isotype control antibody, as shown, at the times indicated. *Gadd45b*$^{+/+}$: anti-CD8 (n=9), isotype (n=7); *Gadd45b*$^{-/-}$: anti-CD8 (n=9), isotype (n=4).

(D) Images of representative tumours from (C) at day 20.

(E) IHC analysis showing the percentage of positive areas per field at 400x of the indicated proinflammatory and antiinflammatory activation markers in the tumours from (B).

(F) Relative luminescence units (RLU) of intraperitoneal ID8-Luc ovarian tumour allografts in *Gadd45b*$^{+/+}$ (n=10) and *Gadd45b*$^{-/-}$ (n=10) mice at the times shown after tumour cell injection.

(G) Bioluminescence images of representative mice from (F) presented as a pseudocolor scale, whereby red and blue denote the highest and lowest photon flux, respectively.

(H) FACS analysis showing the percentage of the indicated intratumoural immune cell populations in *Gadd45b*$^{+/+}$ (n=12) and *Gadd45b*$^{-/-}$ (n=13) mice 60 days after ID8-Luc tumour cell injection.

(I) FACS analysis showing the percentage of CD11b^{+} and F4/80^{+} double positive TAMs expressing high MHC-II levels (MHC-II^{high}) in ID8-Luc tumours from (H).

(J) FACS analysis showing the median MHC-II fluorescence intensity of $CD11b^+$ and $F4/80^+$ double positive TAMs in ID8-Luc tumours from (H).

(H-J) Boxes span between the highest values of the first and third quartiles; whiskers extend to the highest and lowest values within 1.5x of the inter-quartile range. Lines within boxes denote medians.

(K and L) qRT-PCR showing the relative mRNA levels of the indicated proinflammatory activation markers (K) and immune checkpoint molecules (L) in $CD11b^+$ TAMs from *Gadd45b*$^{+/+}$ (n=22) and *Gadd45b*$^{-/-}$ (n=10 or n=12) mice 10 weeks after ID8-Luc cell injection.

(A-C, E, F, K and L) Values denote means ± SEM.

(A-C, E, F, and H-L) *, $p<0.05$; **, $p<0.01$; ***, $p<0.001$.

See also Figure S5.

Figure 6. *Gadd45b* Loss Increases Proinflammatory Macrophage Activation by Enhancing p38 Signalling

(A) qRT-PCR showing the relative mRNA levels of the indicated proinflammatory and antiinflammatory genes in BMDMs from *Gadd45b*$^{+/+}$ and *Gadd45b*$^{-/-}$ mice after a 24-hr co-culture with MCA-203 cells.

(B) qRT-PCR showing the relative mRNA levels of the indicated proinflammatory, NF-κB-regulated and immune checkpoint molecule-coding genes in BMDMs from *Gadd45b*$^{-/-}$ and *Gadd45b*$^{+/+}$ mice after a 4-hr (*Nfkbia, Tnfaip3 and Gadd45b*) or 12-hr (all other genes) stimulation with LPS and IFNγ.

(C) qRT-PCR showing the relative mRNA levels of the indicated antiinflammatory genes after a 26-hr stimulation with IL-4 and IL-13.

(D and E) Western blots showing total and phosphorylated (P) proteins in *Gadd45b*$^{+/+}$ and *Gadd45b*$^{-/-}$ BMDMs after stimulation with LPS and IFNγ for the times indicated. β-actin is shown as loading control.

(F) qRT-PCR showing the relative mRNA levels of the indicated proinflammatory genes in *Gadd45b*$^{-/-}$ BMDMs left untreated (-) or treated with LPS and IFNγ (+) for 12 hr in the presence (+) or absence (-) of the p38 inhibitor, Vx745 (20 μM).

(A-C and F) Values denote means ± SEM (A, B [top] and F, n=4; B [bottom] and C, n=3). *, p<0.05; **, p<0.01; ***, p<0.001.

See also Figure S6.

Figure 7. Suppression of Oncogenesis by Macrophage-Specific *Gadd45b* Deletion

(A) The targeting strategy for generating the loxP-flanked *Gadd45b* allele (*Gadd45b*^{F}).

(B) PCR detecting the wild-type (*Gadd45b*$^{+}$), *Gadd45b*^{F} or excised (*Gadd45b*$^{\Delta}$) *Gadd45b* alleles in the indicated tissues from *Gadd45b*$^{+/+}$ ($^{+/+}$), *Gadd45b*$^{+/F}$ ($^{+/F}$), *Gadd45b*$^{F/F}$ ($^{F/F}$) or *Gadd45b*$^{F/F}$;*LysM-cre* ($^{\Delta M/\Delta M}$) mice.

(C) qRT-PCR showing the relative *Gadd45b* mRNA levels in the indicated tissues isolated from *Gadd45b*$^{F/F}$ ($^{F/F}$) or *Gadd45b*$^{F/F}$;*LysM-cre* ($^{\Delta M/\Delta M}$) mice.

(D) Volumes of subcutaneous MCA-203 fibrosarcoma allografts in *Gadd45b*$^{\Delta M/\Delta M}$ (n=9) and *Gadd45b*$^{F/F}$ (n=8) mice at the times shown.

(E) Images of representative tumours from (D) at day 21.

(F) Summary of the cell injection schedule used in (G and H).

(G) RLUs of intraperitoneal ID8-Luc ovarian tumour allografts in *Gadd45b*$^{+/+}$ mice at the times indicated after intraperitoneal injection of *Gadd45b*$^{+/+}$ (n=9) or *Gadd45b*$^{-/-}$ (n=12) BMDM pools.

(H) Bioluminescence images of representative mice from (G) presented as a pseudocolor scale as in Figure 5G.

(I) Schematic representation of the oncogenic function of Gadd45β in macrophages.

(C, D, and G) Values denote means ± SEM. *, $p<0.05$; **, $p<0.01$.

See also Figure S7.

Figure 1

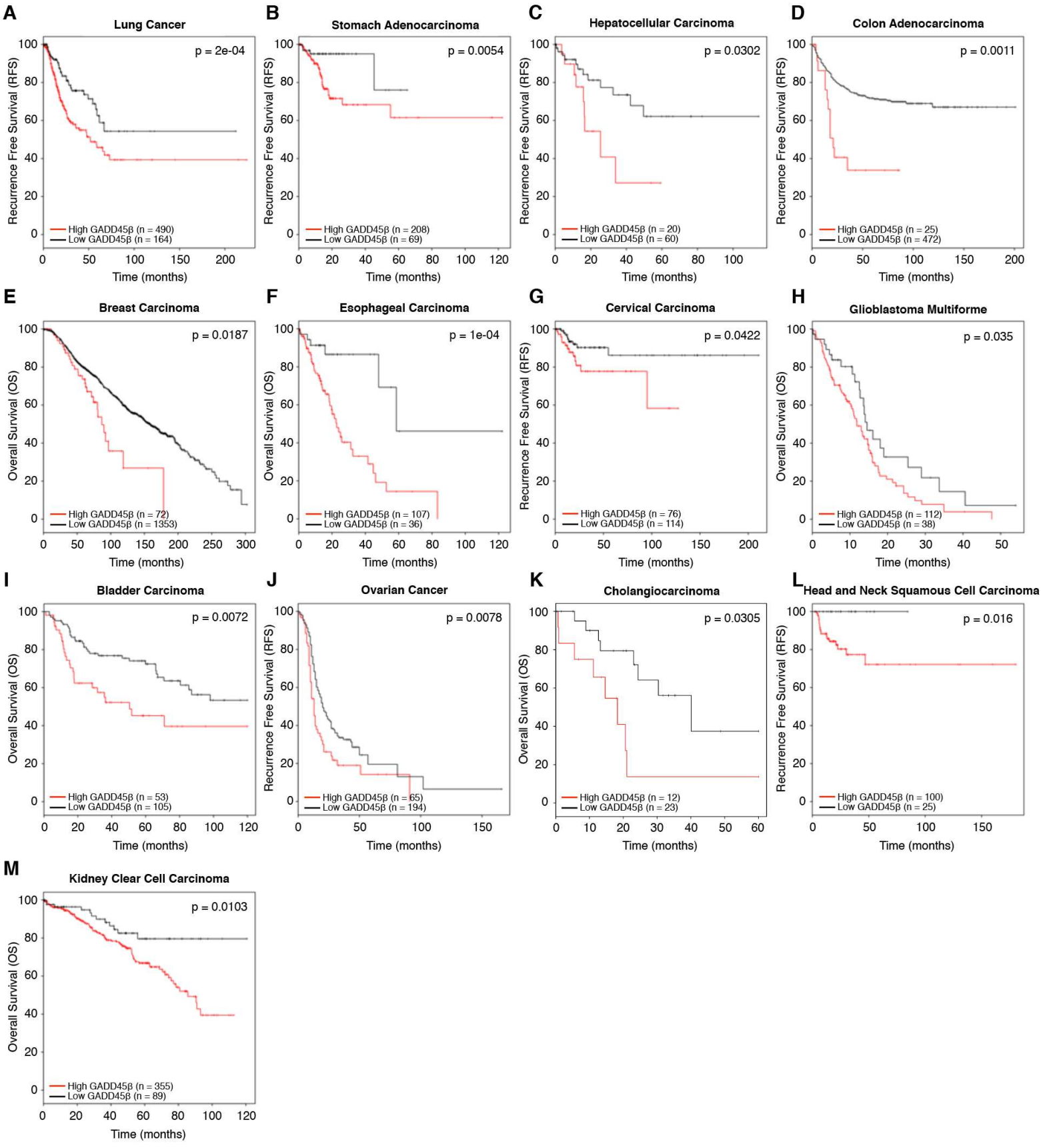

Figure 2

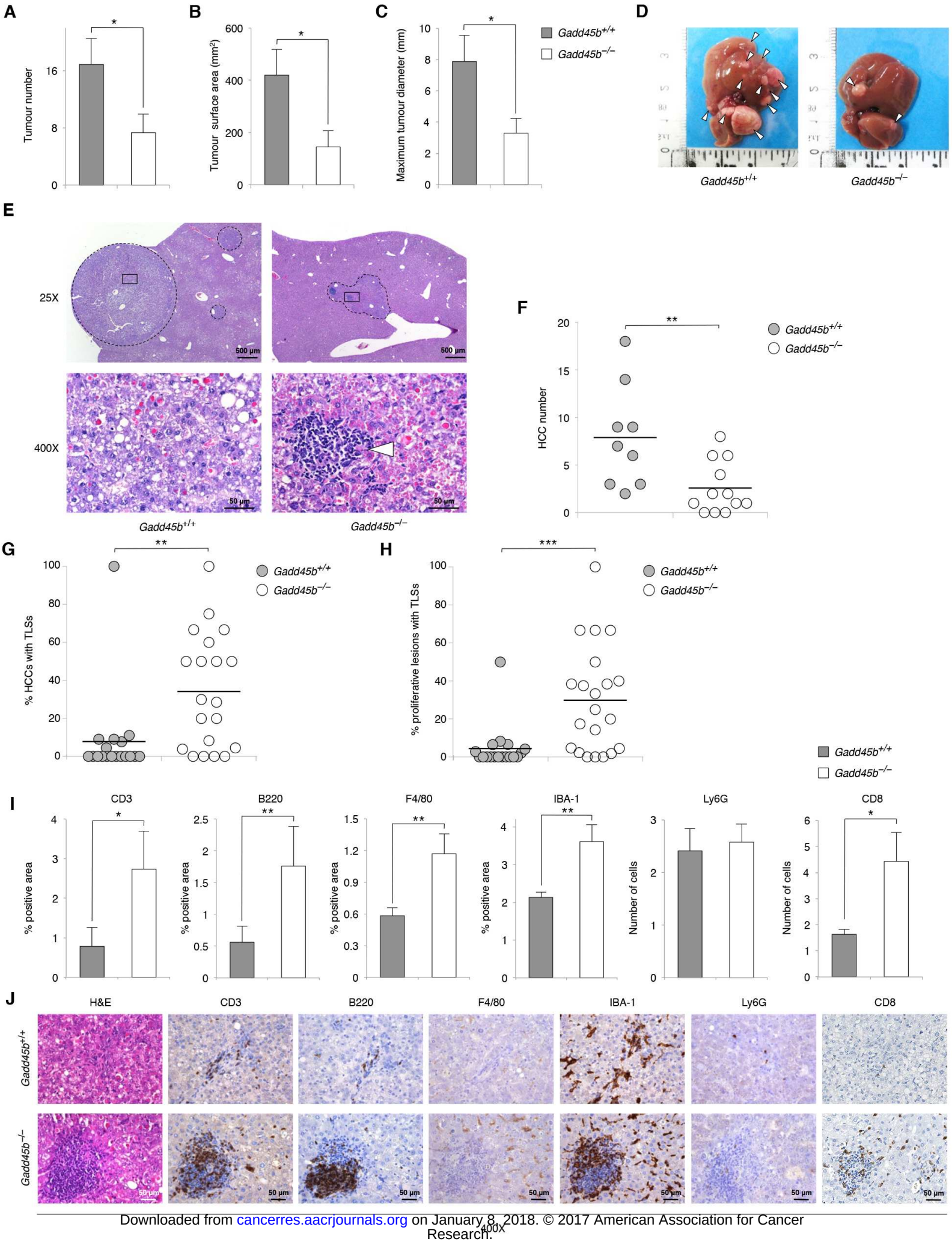

Figure 3

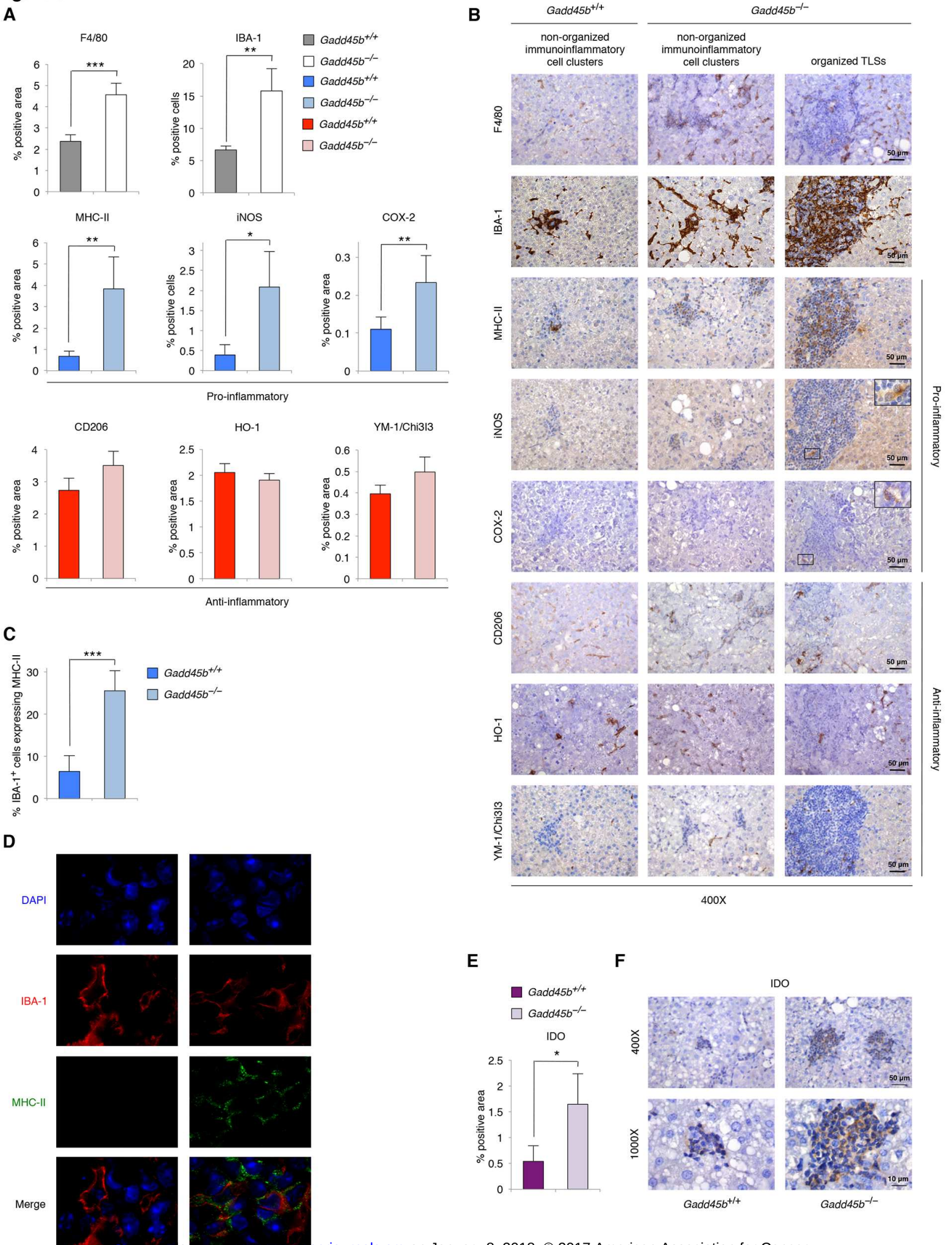

Figure 4

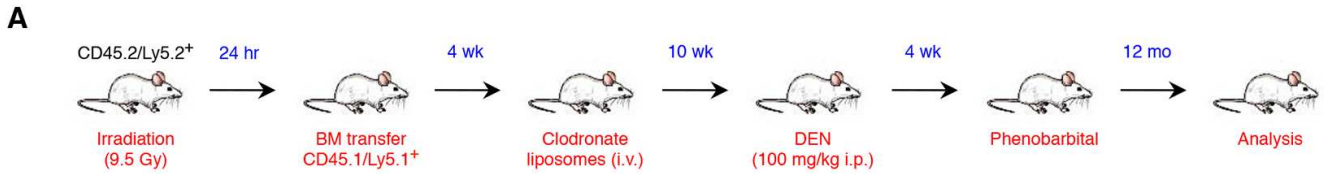

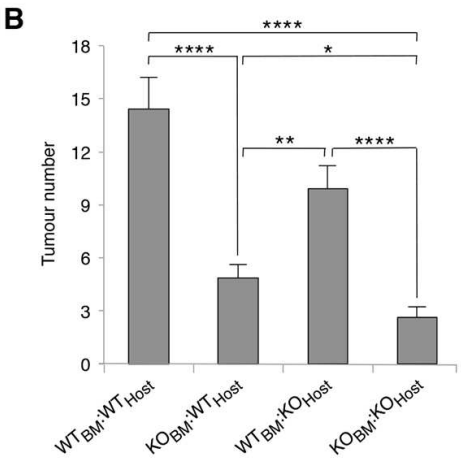

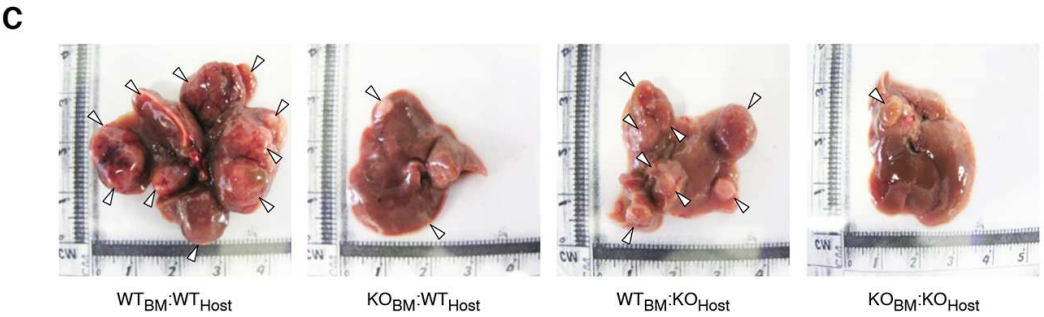

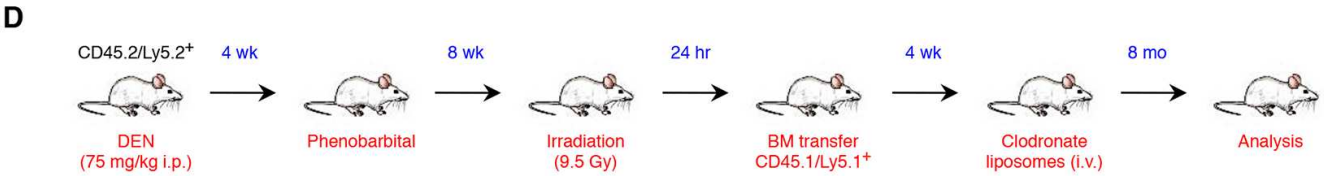

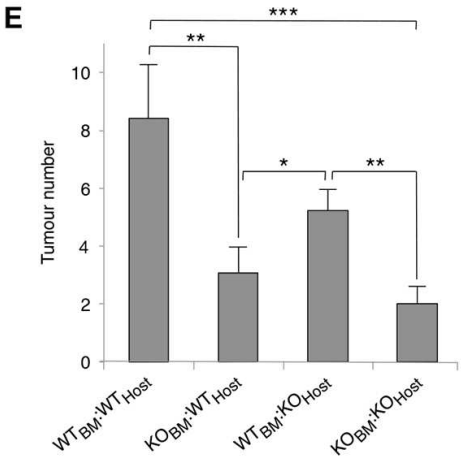

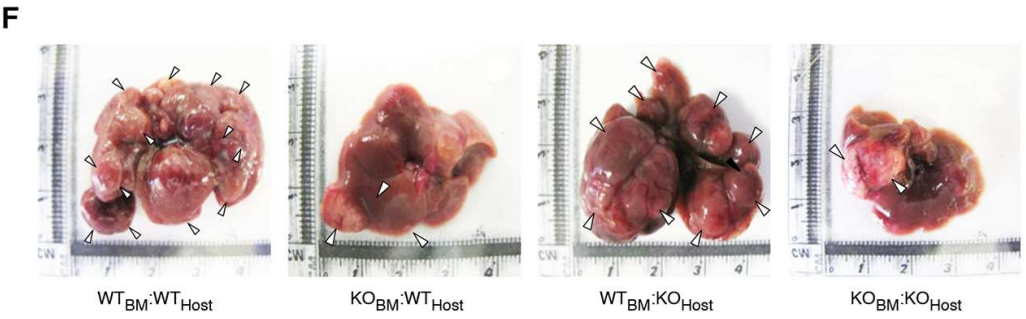

Figure 5

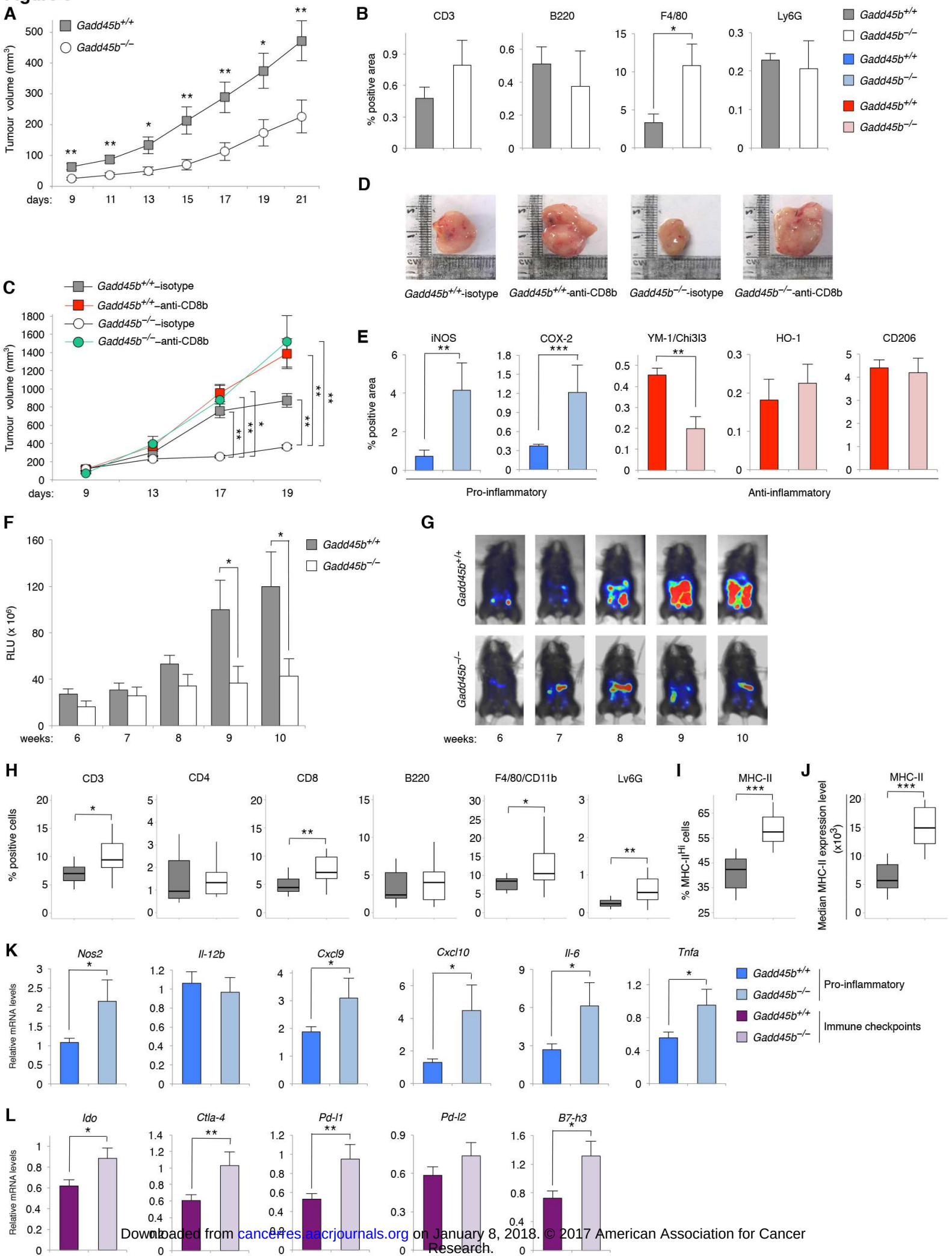

Figure 6

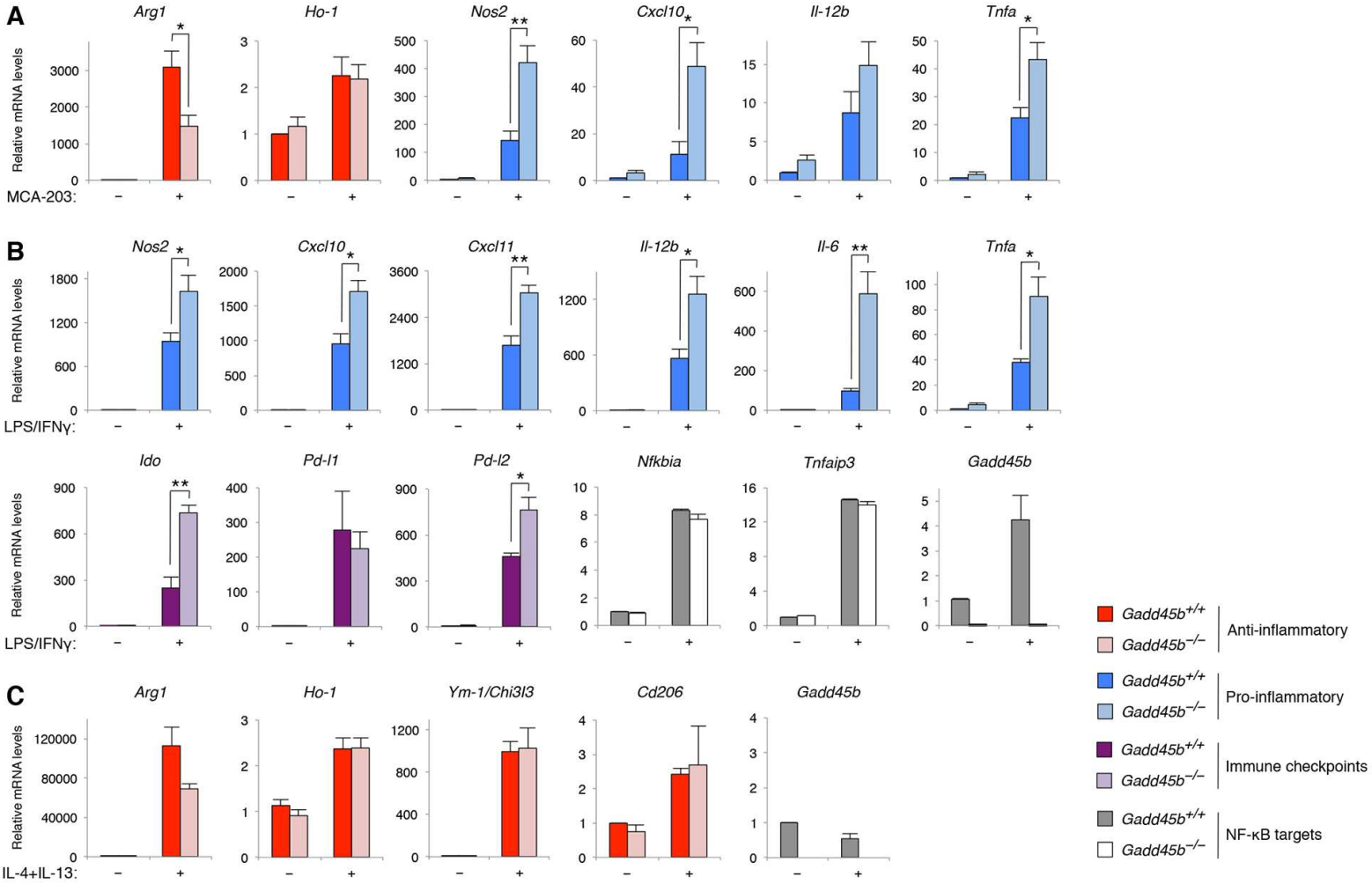

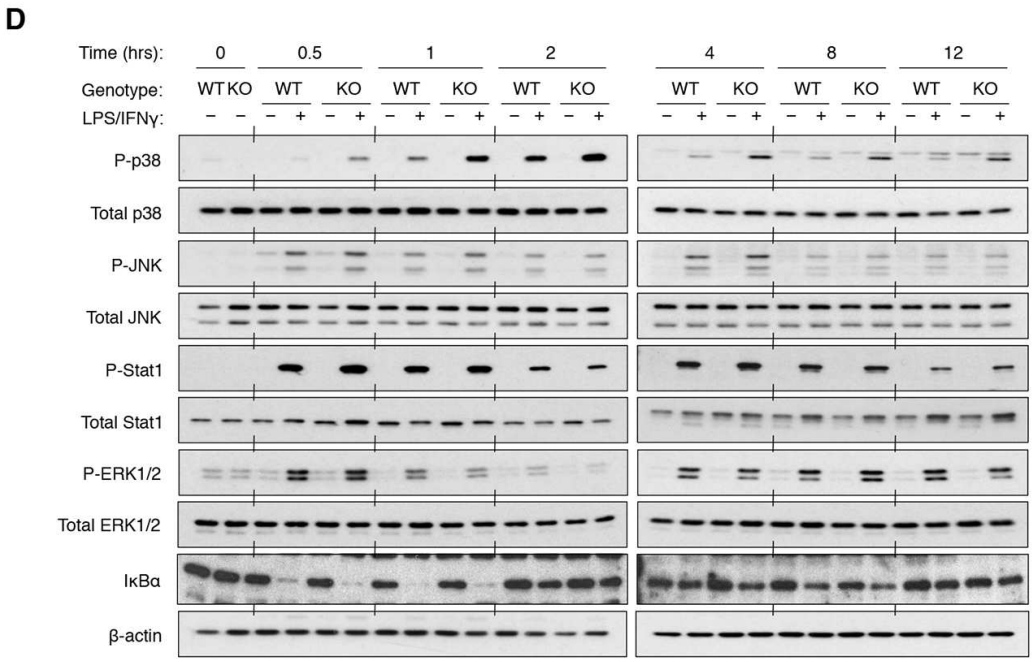

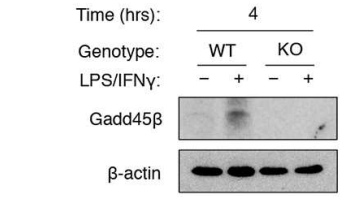

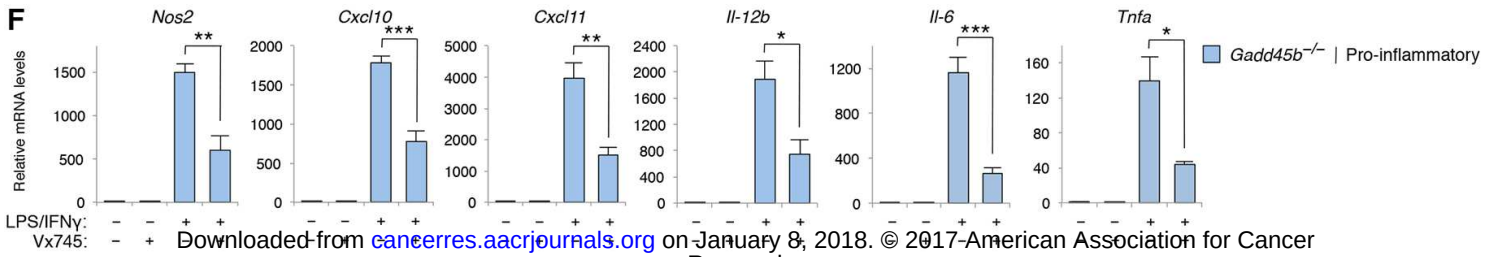

Figure 7

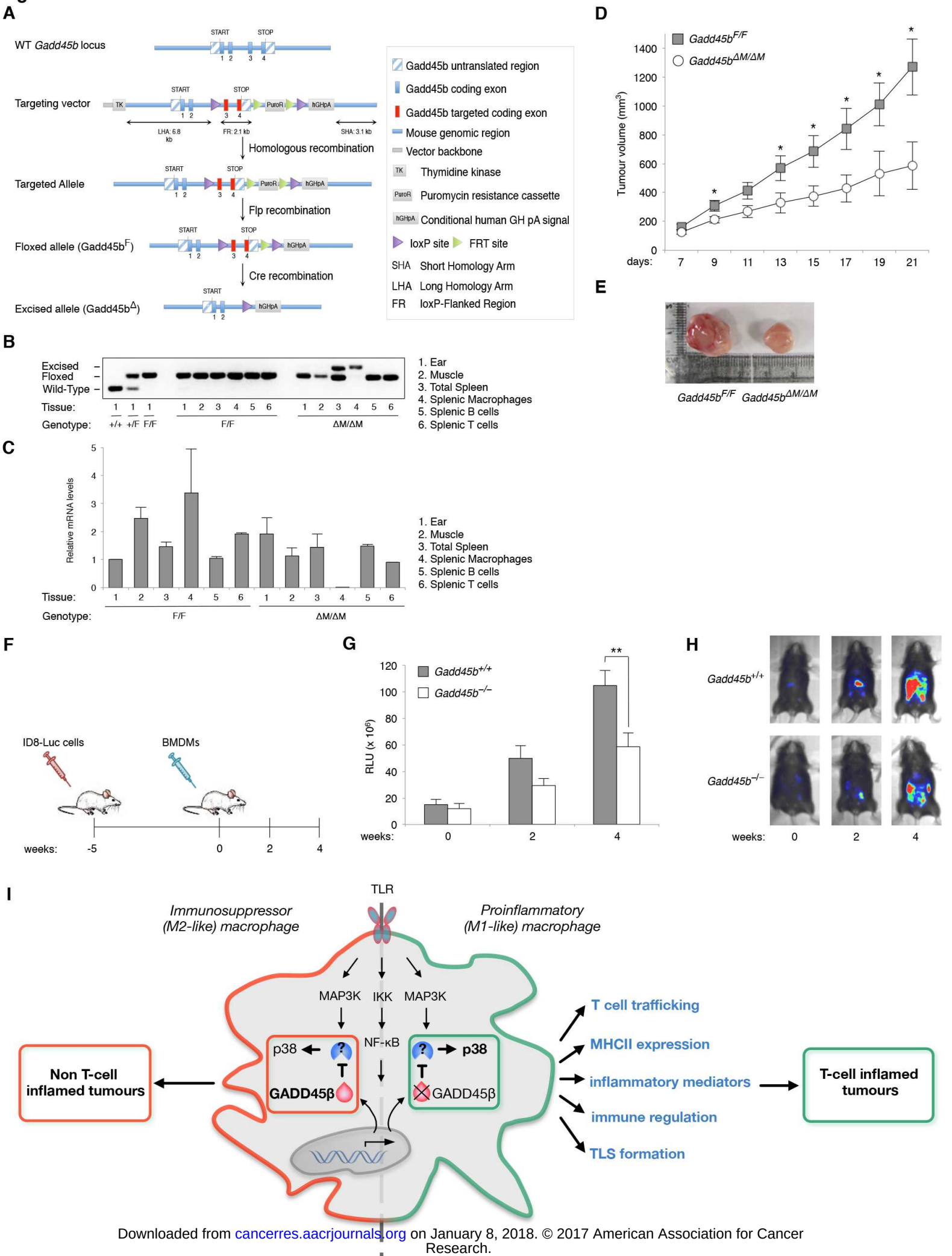

AACR American Association for Cancer Research

Cancer Research

The Journal of Cancer Research (1916–1930) | The American Journal of Cancer (1931–1940)

GADD45β loss ablates innate immunosuppression in cancer

Daniela Verzella, Jason Bennett, Mariafausta Fischietti, et al.

Cancer Res Published OnlineFirst December 26, 2017.